Diyala Journal of Engineering Sciences

Journal homepage:https://djes.info/index.php/djes

ISSN: 1999-8716 (Print); 2616-6909 (Online)

Fractional-Order Direct Power Control of a Doubly Fed Induction Generator-Based Wind Turbine Using Rooted Tree Optimization

Habib Benbouhenni[1*], Adil Yahdou[2], Dalal Zellouma[3], Nicu Bizon[4]

[1]Department of Electrical Engineering, Faculty of Technology, Hassiba Benbouali University of Chlef, Chlef, Algeria.
[2]Department of Electrical Engineering, Faculty of Technology, Laboratoire Génie Electrique et Energies Renouvelables (LGEER), Hassiba Benbouali University of Chlef, Chlef, Algeria.
[3]University of El Oued, P.O. Box789, El Oued, Algeria.
[4]The National University of Science and Technology POLITEHNICA Bucharest, Pitești University Centre, 110040 Pitesti, Romania.

ARTICLE INFO

Article history:
Received: 26/11/2025.
Revised: 26/03/2026.
Accepted: 11/06/2026.
Available online: 15/06/2026.

Keywords:
Power quality
Fractional-order proportional-integral controller
Rooted tree optimization algorithm
Feedback technique
12-sector Direct power control
Pulse Width Modulation
Multi-rotor wind energy conversion system

ABSTRACT

This paper presents a novel control strategy aimed at improving power quality and operational stability in a multi-rotor wind energy conversion system based on a Doubly Fed Induction Generator (DFIG). Conventional Direct Power Control (DPC) techniques often suffer from significant active and reactive power ripples, variable switching frequency, and limited robustness under parameter uncertainties and changing wind conditions. To overcome these drawbacks, a feedback-based Fractional-Order Proportional–Integral (FOPI) controller is integrated into the DPC scheme. The controller parameters are optimally tuned offline using the Rooted Tree Optimization (RTO) algorithm to achieve enhanced dynamic performance and robust operation. The proposed control approach is implemented on the machine-side converter, where instantaneous power estimation is employed to determine the control error, while Pulse Width Modulation (PWM) is used to generate the switching signals and regulate converter operation. By combining the flexibility of fractional-order control with the optimization capability of the RTO algorithm, the proposed method effectively improves power tracking accuracy and reduces system oscillations. To evaluate its effectiveness, the developed strategy is compared with the conventional 12-sector DPC method under various operating conditions. Simulation results obtained using MATLAB/Simulink demonstrate that the proposed controller significantly decreases power and stator current ripples, enhances transient and steady-state responses, and provides superior robustness against disturbances and parameter variations. Consequently, the proposed DPC-FOPI-RTO scheme contributes to improved energy quality, increased system reliability, and better overall performance of DFIG-based wind energy conversion systems.

1. INTRODUCTION

The Wind energy (WE) has emerged as a pivotal contributor to contemporary power generation, attributable to its sustainability and escalating global demand [1]. Among wind turbine (WT) technologies, doubly-fed induction generator (DFIG)-based systems are widely used because of their efficiency, controllability, and cost-effectiveness [2, 3]. However, the integration of DFIG-based WE systems into the electrical grid introduces significant challenges, particularly in maintaining power quality (PQ) under variable wind and grid conditions [4]. Fluctuations in wind speed (WS) and grid disturbances have been shown to cause voltage and current distortions, increased harmonic content, and instability. These phenomena have a deleterious effect on the reliability and performance of the power system [5].

To address these challenges, various control strategies have been developed for enhancing PQ in DFIG-based systems. Conventional proportional-integral (PI) controllers are frequently employed in direct power control (DPC) due to their simplicity and ease of implementation. However, PI controllers frequently exhibit suboptimal dynamic performance during grid disturbances and demonstrate a deficiency in resilience to system parameter variations. In addition, conventional DPC methods can generate significant power ripples and harmonic distortions, which limit their effectiveness in real-world WT applications. Recent advances in control theory have introduced fractional-order controllers as a promising alternative, as they offer memory and hereditary properties that improve adaptability and robustness. When combined with feedback-based techniques, fractional-order controllers can enhance stability and power regulation, particularly in multi-rotor WT (MRWT) systems where interactions between rotors add complexity to control.

*Corresponding author's E-mail: habib0264@gmail.com
DOI: 10.24237/djes.2026.19206

In light of the aforementioned challenges, the present study puts forth a novel control strategy with the objective of enhancing the fineness of the electrical power generated by DFIG-based MRWT systems. The proposed approach utilizes an FO-PI regulator integrated with a feedback technique within a DPC framework. By implementing this strategy exclusively at the machine's inverter, the system achieves enhanced robustness, reduced power fluctuations, and improved grid compatibility. The proposed method is evaluated through MATLAB simulations, demonstrating its effectiveness in maintaining stable operation and high-performance power delivery. This work makes a significant contribution to the ongoing development of advanced power control strategies for renewable energy applications. It focuses particularly on enhancing the reliability and efficiency of WE systems (WES).

In [6], the authors put forth a proposal for a neural network-based field-oriented control (FOC) for a DFIG in a variable-speed WE system (WES). Their approach replaces traditional PI regulators with an artificial neural network (ANN) trained using a backpropagation controller (BC). This enhances system performance, particularly in transient conditions, by reducing overshoot and improving response time. While the method offers greater robustness and adaptability, it also introduces increased computational complexity and requires offline training. Simulations validate the ANN-based control, demonstrating its superiority over PI-based FOC.

Reference [7] presents a hybrid control strategy for a DFIG-based WT system, integrating two hybrid controllers: an ANN with PID and an ANN with predictive control. These regulators regulate DC-link voltage, rotor power, and system frequency, improving response time and system stability while mitigating power fluctuations. The approach enhances robustness and adaptability but introduces computational complexity and tuning challenges. The findings substantiate the hypothesis that the system exhibits superior performance in comparison to conventional methodologies, particularly in scenarios involving grid-linked and islanded modes of operation.

In [8], the authors suggest a new way to improve the low-voltage ride-through (LVRT) capability of a wind farm using DFIG technology. The approach modifies the DPC method by adaptively adjusting active and reactive power (*Ps* and *Qs*) reference values during voltage dips. It employs a voltage dip index (VDI) and optimizes PI regulator parameters using the imperialist competitive algorithm (ICA). Advantages include reduced DC-link voltage fluctuations and rotor overcurrent, while challenges involve complexity and parameter tuning. Simulations validate the method's effectiveness in improving LVRT performance.

In [9], the authors present a WE conversion system (WECS) based on a DFIG and advanced nonlinear control techniques to address PI regulator limitations. Three strategies are implemented for both rotor-side and grid-side converters (RSC and GSC): fuzzy sliding mode control (FSMC), second-order sliding mode controls (SOSMCs), and integral backstepping command (BC). Results show that SOSMC provides superior robustness and tracking accuracy while minimizing chattering. The study highlights the strength of these regulators under parameter variations and disturbances.

In [10], the authors suggest a new plan for controlling direct torque in WT systems using a modified rotor flux-estimated direct torque control (DTC) scheme for DFIG-based WT systems. By employing a fractional-order PID (FPID) regulator, the method decouples torque and flux control, mitigating high ripple issues in conventional DTC. Using rotor voltage, current, and speed measurements to estimate electromagnetic torque, the strategy improves active/reactive power control, DC-link voltage stability, and line current quality, as validated through MATLAB/Simulink simulations.

In [11], the authors introduce a nonlinear BC approach for a DFIG-based WE system. By integrating vector control with BC, the method effectively regulates rotor currents and mechanical speed to optimize power generation. MATLAB/Simulink simulations confirm its robustness, demonstrating improved stability and dynamic response compared to a conventional PI regulator, even under parameter variations. The study shows that the new algorithm works well to improve WE conversion.

The study of PQ in renewable energy systems, particularly in DFIG-based MRWT systems, remains a critical area of research. Despite significant advancements in power control strategies, several research gaps and challenges persist, hindering the full potential of these systems in grid-connected applications. This section highlights key research gaps and challenges associated with PQ enhancement, control strategies, and system robustness.

Traditional PI regulators are often used in DPC in DFIG-based systems. However, these regulators have many problems, including:

- Limited adaptability: PI regulators often struggle with system parameter variations, affecting their performance under fluctuating wind conditions.
- Poor transient response: During grid disturbances, PI controllers fail to provide optimal performance, leading to significant power ripples and instability.
- Inability to mitigate harmonics effectively: Conventional DPC techniques introduce harmonic distortions, affecting PQ and efficiency.

These limitations necessitate the exploration of advanced control techniques that can enhance system adaptability and robustness.
In the work [12], the author used a robust indirect FOC (IFOC) for a squirrel-cage induction generator (SCIG) in a WE conversion system (WECS). The method incorporates artificial intelligence (AI) for speed estimation, enabling sensorless maximum power tracking (MPPT). Advantages include enhanced reliability, improved dynamics, and suitability for commercial applications. However, limitations involve computational complexity and dependence on AI model accuracy for real-time performance. Table 1 illustrates various suggested solutions for enhancing power control in WE systems.

Table 1. Some research article addressing the control of WE systems

Ref.	Strategy	Generator	Contributions	Limitations
[13]	- Employing adaptive PI controllers for dynamic tuning. -Using flux differential terms to improve transient response. -Achieving coordinated dynamic control of DFIG power during commutation failures.	1.5 MW DFIG	This paper presents a novel joint RSC-GSC control strategy for DFIGs, enhancing fault ride-through by dynamically coordinating reactive power support and absorption. It improves system stability during DC commutation-induced cascading voltage failures using adaptive current reference and flux feedback.	The strategy relies heavily on accurate flux and current measurements, which may be sensitive to noise or parameter mismatch. Also, its effectiveness is demonstrated only in simulation; real-world validation under diverse grid conditions and hardware constraints is still needed.
[14]	- Using a modified switching table (MST) with four inputs (torque error, flux error, flux sector, and mechanical slip).	7.5 kW DFIG	The present work introduces a 12-sector DTC strategy, accompanied by a modified switching table for RSC control of DFIGs. The device has been shown to enhance torque and flux regulation, reduce total harmonic distortion (THD), and ensure stable operation across all WT modes, including over speed and super-synchronous conditions.	The method is validated only through simulation, not real hardware. Performance depends on accurate flux, torque, and slip estimation. Additionally, integrating the control strategy into real-time systems could pose realization complexity despite its theoretical simplicity.
[15]	- Neural sliding mode control (SMC). - A recurrent high order neural network (RHONN) identifier. - The following study will examine an extended Kalman filter (EKF) for online training of the RHONN.	1.5 MW DFIG	This work proposes a delay-compensated neural SMC for DFIG-based WTs using a recurrent high order ANN and EKF. It enhances robustness, accuracy, and convergence despite measurement delays and parameter uncertainties.	The proposed controller is only validated through simulations, not hardware. Its performance depends on correct parameter tuning and the ANN training quality. Real-world disturbances, sensor noise, and delay estimation errors could reduce effectiveness or complicate implementation.
[16]	Fuzzy logic (FL) control	1.8 MW permanent magnet synchronous generator (PMSG)	This paper proposes a novel FL-based DC-link voltage control strategy that adaptively adjusts the low-pass filter (LPF) time constant to enhance power smoothing in PMSG-based WT systems, with improved system stability ensured through transfer function analysis and parameter tuning.	- Complexity. - High cost. - Difficulty of completion.
[17]	Application of sliding mode theory	1.5 MW DFIG	- Introduced Variable Gain STA for power command. -Enhanced performance over conventional and third-order SMC.	- Conventional PI controller struggles with parameter changes and WS variations. - Chattering phenomenon occurs in SMC.
[18]	Artificial intelligence techniques	7.5 kW DFIG	- Introduces FL and ANN control techniques. - Reduces power ripples and improves AC grid energy quality.	- Conventional DPC (C-DPC) limitations in WTs. - PQ and efficiency issues in C-DPC.

Even though there have been improvements, there are still research needs in the design of strong and simple control methods for DFIG-based MRWT systems. In particular, there is a need for a control strategy that can effectively reduce power ripples and improve PQ while maintaining robustness under varying wind conditions and grid disturbances. Conventional PI-based DPC methods still struggle with limited adaptability, poor transient response, and insufficient harmonic mitigation. Therefore, there is a clear need for an advanced yet implementable control approach that can overcome these limitations.

This paper presents a new method for improving the performance of DFIG-based MRWT systems. The method uses a fractional-order feedback proportional-integral regulator (FO-FPI). The regulator gains are optimized offline using the rooted tree optimization (RTO) algorithm, which enhances robustness and accuracy in power regulation. The proposed method is applied only to the machine-side converter, simplifying implementation while maintaining effective control. The approach relies on power estimation for error calculation and uses pulse-width modulation (PWM) to drive the inverter. MATLAB/Simulink simulations are used to evaluate the performance of the proposed strategy. The results show that the strategy improves power and current quality, reduces power oscillations, and lowers THD compared with conventional 12 sectors DPC (12-DPC) methods.

The main contributions of this work are summarized as follows: (1) development of a novel DPC strategy for DFIG-based multi-rotor wind systems, (2) integration of a fractional-order feedback PI regulator optimized via rooted tree optimization, (3) implementation of the control strategy on the machine-side converter for simplified operation, (4) use of power estimation to improve control accuracy, and (5) demonstration of improved PQ and robustness through simulation results.

The remainder of this paper is organized as follows. Section 1 introduces the research background and motivation. Section 2 presents the proposed energy system and its main components. Section 3 describes the proposed nonlinear regulator design. Section 4 details the suggested DPC algorithm. Section 5 discusses implementation considerations and computational complexity issues, while Section 6 provides a summary of the computational complexity analysis. Section 7 presents and evaluates the simulation results. Section 8 investigates the trade-off between robustness and response time. Section 9 outlines potential improvements to further enhance system performance. Section 10 discusses the obtained results and their implications. Section 11 addresses the limitations of the proposed approach and suggests directions for future work. Finally, Section 12 concludes the paper and highlights prospective research avenues.

2. PROPOSED ENERGY SYSTEM

The proposed energy system for this study is predicated on the utilization of WE as the primary source of electricity generation. The system under consideration is predicated on a turbine (MRWT), a feature that confers upon it considerable significance within the domain of energy. The utilization of this system has the potential to mitigate the effects of global warming and substantially reduce the costs associated with electricity production and consumption. In addition to the implementation of an MRWT, this system utilizes a DFIG generator to facilitate the conversion of energy output from the MRWT into electrical energy. The studied power system relies on the use of two inverters to power the generator from the rotating part. The generator is directly associated with the grid from the stator part without any intermediary, making this system less expensive and easier to implement. In order to implement the system in MATLAB, it is first necessary to model the main components. The following subsection will delineate the mathematical mode of the MRWT.

2.1 MRWT model

In the field of WTs, MRWTs are a promising solution for power generation. Compared to classical WTs, MRWTs offer a completely different cost, performance, control, durability, and stability [19]. This configuration of WT enables a substantial reduction in the required area for wind farms [20]. Additionally, the implementation of MRWT facilitates the mitigation of the issue posed by strong winds, thereby reducing material and energy dissipation in comparison to conventional WTs [21]. MRWT has been discussed in detail in some research studies [22-24]. In this work, an MRWT containing two WTs is used. The mechanical dynamics of MRWTs are described using the aerodynamic power absorbed by each rotor and the mechanical velocity equation. The total aerodynamic torque is calculated by summing the contribution of each rotor, and the summed inertia is used to model the overall velocity dynamics of the system. The resulting equation is used to study the interaction between aerodynamic torque and electromagnetic torque under varying wind conditions. Each turbine has its own aerodynamic torque, and this aerodynamic torque produced by each rotor is given by Equation (1).

$$T_{a,i} = \frac{P_{a,i}}{w_{a,i}} \tag{1}$$

The velocity dynamics of each rotor are governed by the following mechanical equation:

$$T_{a,i} - T_e - f_i w_{m,i} = J_i \frac{dw_{m,i}}{dt} \tag{2}$$

Where,

J_i: moment of inertia of rotor i.

$T_{e,}$: electromagnetic torque of generator.

fi: viscous friction coefficient of rotor i.

For a two-rotor MRWT system, the total mechanical torque and total inertia can be calculated as follows:

$$\begin{cases} T_{a,tot} = \sum_{i=1}^{2} T_{a,i} \\ J_{a,tot} = \sum_{i=1}^{2} J_{a,i} \end{cases} \quad (3)$$

The combined mechanical velocity dynamics become as follows:

$$T_{a,tot} - T_e - f_{tot} w_{m,avg} = J_{tot} \frac{dw_{m,avg}}{dt} \quad (4)$$

Where, $w_{m,avg}$ is the average mechanical speed of the MRWT system.

On the other hand, the power output of MRWT in this work is written as shown in Equation (5).

$$P_t = P_1 + P_2 \quad (5)$$

In the context of the given equation, the variables P_1 and P_2 represent the generated power of the first and second WT, respectively. The variable P_t, on the other hand, denotes the total power of the MRWT.

The MRWT torque is defined as the sum of the torques of the two WTs. The torque in question is contingent upon the dimensions of each WT and WS. Equation (6) expresses the torque of each turbine forming the MRWT [22].

$$\begin{cases} T_1 = \frac{1}{2\lambda_1^3} . \rho . \pi . R_1^5 . C_p . w_1^2 \\ T_2 = \frac{1}{2\lambda_2^3} . \rho . \pi . R_2^5 . C_p . w_2^2 \end{cases} \quad (6)$$

In the context of this study, R_1 and R_2 represent the blade radius of the two WTs, while ρ denotes the air density. The mechanical speed of the two turbines is indicated by w_1 and w_2, and the tip speed ratio (TSR) of the two WTs is represented by λ_1 and λ_2.

The power gained from wind is related to a factor called the coefficient of power (C_p). This factor is predominantly associated with the dimensions of the WT and the WS. This factor is expressed by Equation (7).

$$C_p(\lambda, \beta) = \frac{1}{\lambda + 0.08\beta} - \frac{0.035}{\beta^3 + 1} \quad (7)$$

Where, β is the pitch angle.

The TSR for each WT is represented in Equation (8).

$$\begin{cases} \lambda_1 = \frac{w_1 . R_1}{V_1} \\ \lambda_2 = \frac{w_2 . R_2}{V_2} \end{cases} \quad (8)$$

The velocity of the initial WT is directly proportional to the WS. However, the velocity of the secondary WT is contingent upon the distance between the two WTs and the WS preceding the primary WT. As indicated in the research conducted in [25], the WS preceding the second WT can be expressed through the utilization of Equation (9).

$$V_2 = V_1 (1 - \frac{1 - \sqrt{(1 - C_T)}}{2} (1 + \frac{2.x}{\sqrt{1 + 4.x^2}})) \quad (9)$$

Where, C_T is the constant coefficient, whose value is equal to 0.9, V_2 is the WS of the turbine 2, and x is the distance between the turbine 1 and turbine 2.

2.2 DFIG model

The Park transform is frequently employed in the modeling of DFIG. This transformation is predicated on the provision of mathematical equations that represent each component of the generator. This modeling has been thoroughly delineated in numerous research works [26-28]. According to the work done in [29], the voltage of the rotor in a Park system can be expressed by Equation (10).

$$\begin{cases} V_{dr} = R_r I_{dr} + \frac{d}{dt} \psi_{dr} - \omega_r \psi_{qr} \\ V_{qr} = R_r I_{qr} + \frac{d}{dt} \psi_{qr} + \omega_r \psi_{dr} \end{cases} \quad (10)$$

Where, I_{qr} and I_{dr} are the currents of the rotor in the d-q reference frame, ω_r is the electrical pulsation of the rotor, ψ_{qr} and ψ_{dr} are the flux of the rotor in the d-q reference frame, V_{qr} and V_{dr} are the voltages of the rotor in the d-q reference frame, and R_r is the rotor resistance.

The stator of the generator can be expressed in Park system according to Equation (11).

$$\begin{cases} V_{ds} = \frac{d}{dt} \psi_{ds} + R_s I_{ds} - \omega_s \psi_{qs} \\ V_{qs} = \frac{d}{dt} \psi_{qs} + \omega_s \psi_{ds} + R_s I_{qs} \end{cases} \quad (11)$$

Where, I_{qs} and I_{ds} are the currents of the rotor in the d-q reference frame, ψ_{qs} and ψ_{ds} are the flux of the stator in the d-q reference frame, V_{qs} and V_{ds} are the voltages of the stator in the d-q reference frame, ω_s is the electrical pulsation of the stator, and R_s is the stator resistance.

Using Equations (10) and (11), the generator powers can be calculated. These powers are listed in Equation (12).

$$\begin{cases} P_s = \frac{3}{2} (V_{ds} I_{ds} + V_{qs} I_{qs}) \\ Q_s = \frac{3}{2} (V_{qs} I_{ds} - V_{ds} I_{qs}) \end{cases} \quad (12)$$

Where, Ps is the active power and Qs is the reactive power.

Equation (13) expresses the flux in the rotating part of the generator. This flux is used to estimate the powers [30].

$$\begin{cases} \psi_{dr} = M I_{dr} + L_r I_{dr} \\ \psi_{qr} = M I_{qr} + L_r I_{qr} \end{cases} \quad (13)$$

Where, M is the Mutual inductance.

The relationship between the stator flux of the generator and the stator current can be expressed by the following Equation (14).

$$\begin{cases}\psi_{ds} = MI_{dr} + L_s I_{ds} \\ \psi_{qs} = MI_{qr} + L_s I_{qs}\end{cases} \quad (14)$$

Where, L_s is the stator inductance.

Using Equations (13) and (14), the torque of the generator can be expressed by Equation (15) [31].

$$T_e = \frac{3}{2} p \frac{M}{L_r} (I_{dr}.\psi_{qs} - I_{qr}.\psi_{ds}) \quad (15)$$

Where, T_e is the torque, p is the number of pole pairs, L_r is the rotor inductance.

Equation (15) plays an important role in generator operation. This equation is used to derive the speed evolution equation. Equation (16) is used to study the speed evolution. Equation (16) controls generator operation.

$$T_e - T_r = J \cdot \frac{d\Omega}{dt} + f \cdot \Omega \quad (16)$$

Where, J is the inertia, f is the viscous friction, and Ω is the Mechanical rotor speed.

In the following section, an examination will be conducted regarding a novel controller for the management of electrical power, accompanied by a delineation of its primary benefits.

3. PROPOSED NONLINEAR REGULATOR

A plethora of regulatory frameworks have been proposed within the domain of control. These regulators can be categorized into three distinct classifications: nonlinear regulators [32], linear regulators [33], and hybrid regulators [34]. The PI regulator is a prominent example of such a regulator, maintaining its popularity due to its ease of realization and configuration [35]. This regulator has been employed to optimize both the DPC and DTC algorithms [36, 37]. The utilization of a PI (proportional-integral) regulator has been demonstrated to result in a substantial enhancement in performance when compared to hysteresis comparator regulators. However, the PI regulator exhibited results that were not commensurate with those of the BC when operated [38]. Furthermore, the PI regulator exhibited inadequate performance in terms of power ripples when compared to the RST regulator [39]. As indicated in the research conducted in [40], the low robustness of the PI controller is regarded as one of its most substantial drawbacks. In circumstances where system parameters are subject to variation, the PI regulator is observed to be considerably impacted. This phenomenon is evident in the escalation of fluctuation values and the current THD.

A review of the extant literature reveals several proposed solutions to the problems of the PI regulator. The most prominent of these solutions involves the use of other algorithms, such as genetic algorithms [41], synergetic control [42], artificial neural network (ANN) techniques [43], anti-colony optimization [44], super-twisting control [45], and particle swarm optimization [46]. In [47], a dual PI regulator was proposed as a solution to replace the use of a PI regulator in the control area. This approach has proven to be effective; however, it does introduce a greater degree of complexity and an increased number of gains. Conversely, a parallel PI regulator was proposed as a suitable solution to control the operation of an induction motor in [48]. The efficacy of the regulator was demonstrated by its satisfactory performance in terms of response time, fluctuations, overshoot, and current THD. Nevertheless, this approach is not without its drawbacks. The greater the number of gains, the more difficult the implementation, and the more complex the process, the more pronounced these disadvantages become. Consequently, these disadvantages hinder the use of this approach in the future.

In this section, a controller featuring simplicity, high solidity, excellent performance, and ease of realization is designed to replace the use of a PI in control. This designed regulator is heavily based on the PI regulator. It is an improvement on the PI regulator, utilizing feedback techniques, fractional calculus, and the RTO algorithm. Therefore, the RTO algorithm-based fractional-order feedback PI (FO-FPI-RTO) regulator is the proposed solution in this paper to replace the use of PI regulators in the control domain. This approach combines several different strategies, making it highly efficient and effective. This approach is represented in Figure 1.

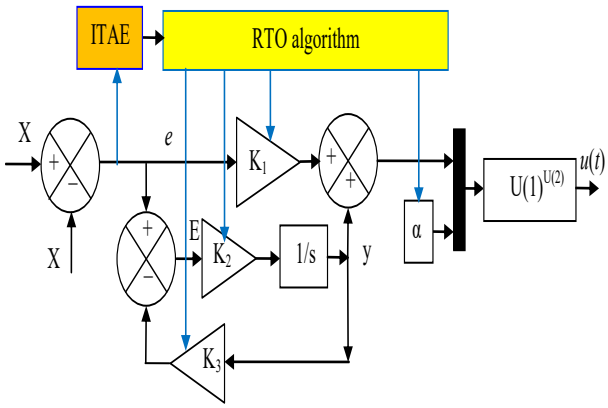

Figure 1. Proposed FO-FPI-RTO regulator.

The determination of the optimal values for the gains of the FO-FPI-RTO regulator is achieved through the utilization of the Integral of Time-weighted Absolute Error. The calculation of the ITAE value is achieved through the utilization of Equation (17). A comprehensive list of the properties of the RTO algorithm utilized in this study is provided in the supplementary file.

$$ITAE = \int_0^\infty t \times |e(t)| \times dt \quad (17)$$

In this designed regulator, the gain values are calculated using the RTO algorithm, as shown in Figure 1. The properties of the RTO algorithm used in this paper are listed in the supplementary file. The values of the obtained optimal gains are also listed in this file. The

implementation of this algorithm has been demonstrated to enhance performance and efficiency. As illustrated in Figure 1, the mathematical model of the novel algorithm is depicted by Equation (18).

$$u(t) = [K_1.e(t) + K_2.\int E(t)dt]^{\alpha} \quad (18)$$

With:

$$E(t) = e(t) - K_3.y \quad (19)$$

Where, α is the fractional-order control, *e*(*t*) is the error, *E*(*t*) is the error of the feedback technique, and K_1, K_2, and K_3 are the gains of the new algorithm.

As indicated in the preceding paragraph, it is posited that the dynamic response of the regulator under review may be controlled and adjusted using the gain values K_1, K_2, and K_3.

Conversely, the efficacy of the novel algorithm is contingent upon the value of α. For the regulator to be considered valid, it is imperative that the value of α does not equal 0. If the value of α takes the value 1, the designed regulator becomes an FPI, where Equation (18) is written as $(u(t) = K_1.e(t) + K_2.\int E(t)dt)$. Therefore, the designed regulator is an FO-FPI-RTO regulator, and the value of α must differ between 1 and 0.So we can say that this designed regulator is two different controls in one regulator, where the transition from one type to another is done by controlling the value α.

The reliability of the aforementioned approach can be substantiated through the utilization of the Bode curve or Lyapunov's theorem. As is known, a fractional-order term improves the system's robustness and smooth convergence due to the memory effect. Furthermore, stability can be ensured when the value of α takes $0 < \alpha \leq 1$.On the other hand, the RTO algorithm only affects the gain selection and does not alter stability, as it operates outside the system. This analysis assumes that the system output is limited, an assumption that holds true for inverter-driven electrical machines.

To facilitate the process of proving stability, Equation (20) is imposed.

$$z(t) = \int E(t).dt \quad (20)$$

The derivation of Equation (20) is written as follows:

$$\dot{z}(t) = E(t) = e(t) - K_3 y(t) \quad (21)$$

Based on Equation (21), the organizer designed in this paper can be written as follows:

$$u(t) = (K_1.e + K_2.z)^{\alpha} \quad (22)$$

For Lyapunov's analysis, it is assumed that the error dynamics of the controlled system can be expressed as follows:

$$\dot{e}(t) = -u(t) \quad (23)$$

This assumption is widely used in power, current, and torque control loops, and allows for a focus on the regulator's stability characteristics.

With:

$$\dot{e}(t) = -(K_1.e + K_2.z)^{\alpha} \quad (24)$$

The candidate Lyapunov function is chosen in this paper as shown in Equation (25).

$$V(e,z) = \frac{1}{2}e^2 + \frac{1}{2}z^2 \quad (25)$$

Based on Equation (25), the following properties can be achieved.

$$\begin{cases} V(e,z) > 0 \; for \; (e,z) \neq (0,0) \\ V(0,0) = 0 \\ V \; is \; radially \; unbounded \end{cases} \quad (26)$$

The time derivative of the Lyapunov function is written as follows:

$$V = e.\dot{e} + \dot{z}.z \quad (27)$$

Substituting $\dot{e}$ and $\dot{z}$, Equation (27) becomes as follows:

$$\dot{V}(t) = -e.(K_1.e + K_2.z)^{\alpha} + z(e - K_3.y) \quad (28)$$

The designed structured stability analysis is performed using the inequality represented by Equation (29).

$$(K_1.e + K_2.z)^{\alpha} \geq C_1|e|^{\alpha} + C_2|z|^{\alpha} \quad (29)$$

With: C_1 and C_2>0

For $0 < \alpha \leq 1$, we obtain:

$$\dot{V} \leq -K_1^{\dot{\alpha}}|e|^{\alpha+1} - K_2^{\alpha}|z|^{\alpha+1} + |z|.|e| + K_3|z| \quad (30)$$

Since:

y(t) is bounded in physical systems (e.g., DFIG-based converters),

All controller gains are positive.

The negative terms dominate for sufficiently large |e| and |z|, yielding:

$$\dot{V} \leq 0 \quad (31)$$

Thus, the closed-loop system is Lyapunov stable, and all signals remain bounded.

For asymptotic stability to occur, the condition $\dot{V} = 0$ must be satisfied, which is only true when:

$$\begin{cases} e(t) = 0 \\ z(t) = 0 \end{cases} \quad (32)$$

By LaSalle's invariance principle, the system trajectories converge to the equilibrium point:

$$\lim_{t \to \infty} e(t) = 0 \quad (33)$$

Therefore, it can be concluded that the closed-loop system is asymptotically stable.

Table 2 compares the controller designed in this paper with some existing controllers in the literature, such as PID and SMC. This comparison focuses on similarities and differences, comparing these controllers in terms of simplicity, gain, robustness, etc. The comparison was based on literature that addressed these various controllers.

Classical PI and PID controllers are simple and easy to implement but suffer from poor robustness and high sensitivity to parameter variations, leading to increased power ripple and current THD. FO-PI controllers improve damping and reduce oscillations through fractional-order integration but introduce additional tuning complexity. On the other hand, SMC provides excellent robustness and fast response; however, it requires accurate system modeling and suffers from chattering, which degrades PQ and complicates implementation in power electronic systems.

The FO-FPI-RTO controller has been proposed as an alternative that offers a balanced compromise between robustness, PQ, and implementation complexity. By incorporating fractional-order memory and nonlinear gain shaping, it achieves low power ripple and THD while avoiding chattering and excessive computational burden. Although its dynamic response is slower than SMC, this trade-off is acceptable for WE systems, where robustness and PQ are prioritized over ultra-fast response.

The strength and efficacy of the regulator suggested in this paper in controlling the power of a DFIG are studied. The following section discusses the use of the regulator in power control in detail, highlighting the key advantages of using this regulator.

Table 2. Comparison between PI, PID, FO-PI, SMC, and FO-FPI-RTO Controllers

Criterion	PI	PID	FO-PI	SMC	FO-FPI-RTO
Control structure	Linear	Linear	Fractional linear	Nonlinear	Nonlinear fractional
Number of gains	2 (K_p, K_i)	3 (K_p, K_i, K_d)	3 (K_p, K_i, α)	≥2 + switching gain	4 (K_1, K_2, K_3, α)
Ease of application	Very easy	Easy	Moderate	Difficult	Moderate
Ease of implementation	Very high	High	Moderate	Low (chattering issue)	Moderate
Need for accurate model	Low	Low	Low–Moderate	High	Low
Use of system mathematical model	Not required	Not required	Partial	Required	Partial
Robustness to disturbances	Low	Low–Moderate	Moderate	Very high	High
Robustness to parameter variations	Low	Low	Moderate	Very high	High
Dynamic response speed	Fast	Faster	Moderate	Very fast	Moderate
Overshoot / oscillations	High	Moderate	Low	Very low	Very low
Susceptibility to machine parameter changes	High	High	Moderate	Low	Low
Current THD	High	Moderate	Low	Very low	Very low
Power ripple	High	Moderate	Low	Very low	Very low
Computational complexity	Very low	Low	Moderate	High	Moderate
Switching frequency	Variable	Variable	Variable	Variable	Fixed (PWM-based)
Chattering phenomenon	No	No	No	Yes	No
Suitability for real-time implementation	Excellent	Excellent	Good	Challenging	Good
Adaptability to renewable systems	Limited	Limited	Good	Good	Very good

4. SUGGESTED DPC ALGORITHM

This section presents the proposed control methodology, including its mathematical model, implementation plan, and detailed operating procedures. This methodology is designed to improve the PQ and stability of a multi-rotor WT system based on a DFIG.

Using the PI regulator-based DPC as a solution for controlling DFIG-based turbine systems. This strategy faces challenges in dealing with the inherent nonlinearity of system dynamics and uncertainties. In addition, the DPC-PI does not produce satisfactory results with regard to PQ and current THD. This necessitates the implementation of a more efficient strategy while preserving the simplicity of the DPC-PI. The FO-FPI-RTO control is a suitable solution for dealing with uncertainties because it relies on several different strategies. In this designed solution, the FPI regulator provides fast dynamic response while maintaining simplicity and ease of control, as well as neural networks. The use of fractional calculus technology leads to high robustness and improved operational efficiency. The use of the RTO algorithm increases system efficiency and reliability, while enhancing accuracy. Consequently, the control approach delineated in this paper addresses the deficiencies and limitations of the DPC-PI. The objective of this study is to develop a control algorithm that utilizes the benefits of multiple strategies to address the significant limitations of renewable energy systems, thereby ensuring sustainability and the provision of high-quality energy.

In managing advanced WE systems, a key challenge is effectively dealing with the nonlinearities, complex dynamics, and inherent uncertainties that affect system operational performance. The FO-FPI-RTO approach

aims to address these challenges through robust power control and high robustness.

In advanced turbine system management, FO-FPI-RTO is a new algorithm that is highly effective against system parameter changes and power fluctuations. Combined with its simplicity and ease of adjustment, this approach is a suitable solution.

The FO-FPI-RTO approach is an evolution of the DPC-PI strategy. In this approach, the power is controlled using two FO-FPI-RTO regulators. These controllers enable the adjustment of voltage in accordance with the power error. In addition to the FO-FPI-RTO regulator, the PWM is utilized to generate the requisite pulses. The PWM was adopted in order to preserve the simplicity and ease of implementation that characterize the DPC-PI.

The FO-FPI-RTO approach relies on power estimation, as in the FO-FPI-RTO approach. Power estimations are performed to estimate a power error. This power error is represented by the inputs of the FO-FPI-RTO regulator, which are used to control the operation of the machine's inverter. It has been demonstrated that the estimation equations utilized in the FO-FPI-RTO are identical to those employed in the DPC-PI.

Figure 2 represents the structural diagram of the FO-FPI-RTO used for power control. As demonstrated in Figure 2, the simplicity, ease of application, ease of implementation, and ease of control are the most prominent features of this algorithm. Additionally, the implementation of this algorithm in complex systems is not contingent upon precise knowledge of the mathematical model under study.

4.1 Flowchart of the Proposed Control Strategy

The proposed control strategy follows the steps shown in Figure 3. First, the network currents and voltages are measured and used to estimate the instantaneous *Ps* and *Qs*. Second, the power errors are calculated relative to the reference values. The FO-FPI controller, whose gains are externally optimized using the RTO algorithm, generates reference voltage signals. These reference signals are then processed by a PWM module to produce switching pulses that reverse the current on the rotor side. The inverter controls the rotor currents and ensures efficient power control; this process is repeated at each sampling moment.

4.2 Working Methodology of the Proposed Algorithm

The proposed method follows the steps below:

- Power Measurement and Estimation

The instantaneous active and reactive powers (*Ps* and *Qs*) are estimated using Clarke transformation and instantaneous power theory.

- Error Calculation

The power errors are calculated as:

$$\begin{cases} e_{Ps} = P_s^* - P_s \\ e_{Qs} = Q_s^* - Q_s \end{cases} \quad (34)$$

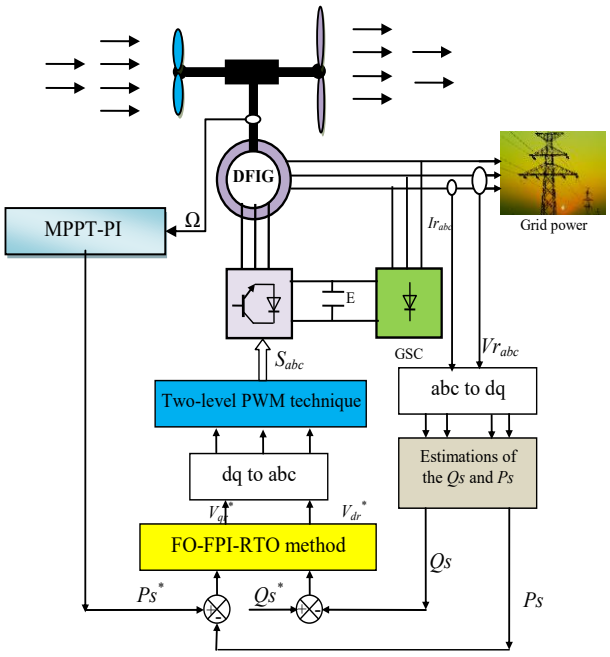

Figure 2. Proposed FO-FPI-RTO technique of DFIG-MRWT.

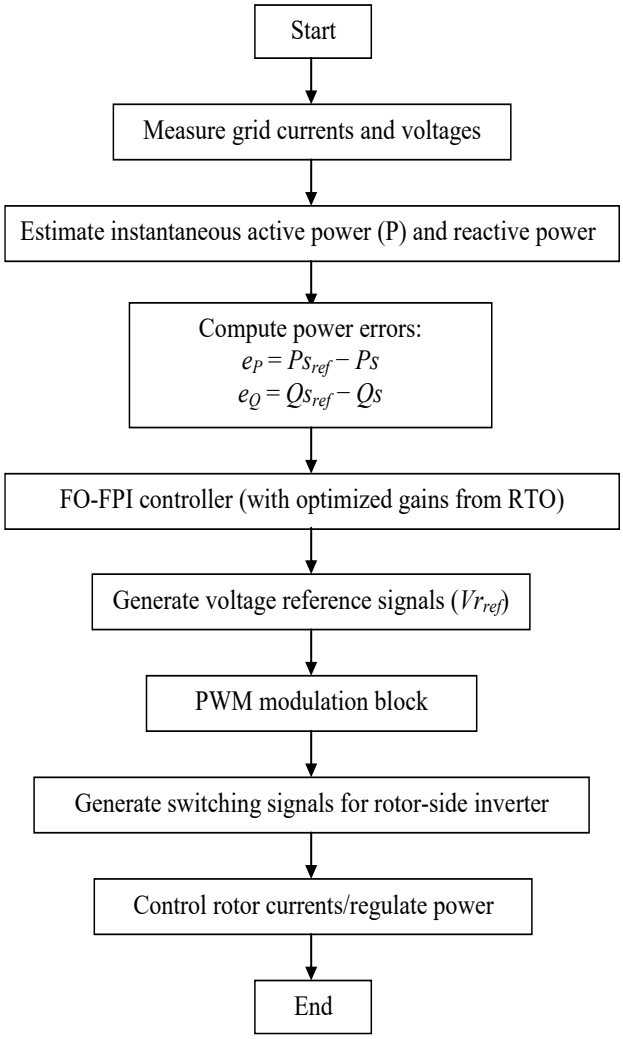

Figure 3. Flowchart of the proposed control strategy based on FO-FPI-RTO controller.

In order to control the power, the flux must first be estimated. To estimate the flux, the voltage and current are measured. Equation (35) is used to estimate the flux in the rotor part [49].

$$\begin{cases} \psi_{r\alpha} = \int_0^t (v_{r\alpha} - R_r i_{r\alpha})dt \\ \psi_{r\beta} = \int_0^t (-R_r i_{r\beta} + v_{r\beta})dt \end{cases} \quad (35)$$

In the same way, the stator flux of the generator is estimated using Equation (36). These fluxes are used to determine the estimated values for the DFIG power.

$$\begin{cases} \psi_{s\alpha} = \int_0^t (-R_s i_{s\alpha} + V_{s\alpha})dt \\ \psi_{r\beta} = \int_0^t (-R_s i_{s\beta} + V_{s\beta})dt \end{cases} \quad (36)$$

As indicated in the research of [50], the estimation of powers can be achieved through the utilization of Equations (37) and (38).The utilization of these equations is estimate on the estimation of the power error.

$$P_s = -\frac{3}{2}\frac{Lm \times (Vs.\psi_{r\beta})}{\sigma \times Ls \times Lr} \quad (37)$$

$$Q_s = -\frac{3}{2}\left(-\frac{Vs.Lm}{\sigma.Ls.Lr}\cdot\psi_{r\alpha} + \frac{Vs}{\sigma.Ls}\cdot\psi_{r\beta}\right) \quad (38)$$

With:

$$\sigma = -\frac{M^2}{L_r L_s} + 1 \quad (39)$$

Where, σ is the dispersion coefficient.

- PWM Generation

The reference signals are compared with a triangular carrier signal to generate PWM pulses for the inverter.

- Converter Control

The inverter switches are controlled to regulate the DFIG rotor currents and thus control the power flow.

- Fractional-Order Control Action

The FO-FPI-RTO controller generates reference voltage signals. Equation (18) is used to represent the power outputs of this controller. The values enumerated in Equation (34) are employed to estimate the reference values for the rotor voltage. The reference value for the direct rotor voltage is calculated using the reactive power error, as outlined in Equation (40). As illustrated in Figure 4, Equation (40) can be represented in a variety of ways.

$$V_{dr}^* = (K_1.e_{Qs} + K_2.\int E(t)dt)^{\alpha} \quad (40)$$

The reference value of the quadrature rotor voltage is determined using Equations (18) and (34), as outlined in Equation (41). The reference value of the quadrature rotor voltage is directly associated with the value of the *Ps* error. As illustrated in Figure 5, the FO-FPI-RTO is employed to ascertain the reference value of the quadrature rotor voltage.

$$V_{qr}^* = (K_1.e_{Ps} + K_2.\int E(t)dt)^{\alpha} \quad (41)$$

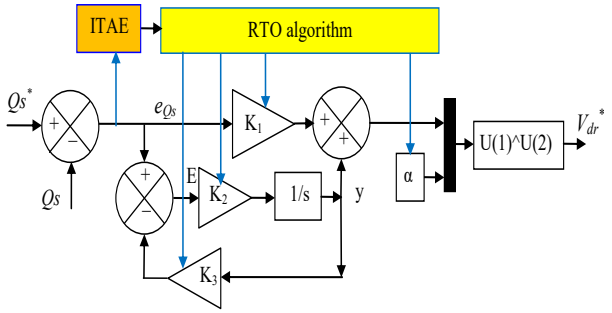

Figure 4. Proposed reactive power controller.

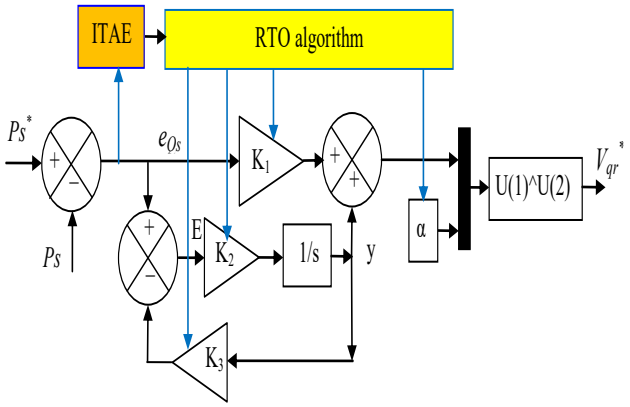

Figure 5. Proposed active power controller.

4.3 RTO Optimization Process (Offline)

The RTO algorithm is used offline to optimize the controller parameters. The process is as follows:

- Define the optimization search space for K_i, K_p, and α.
- Initialize the root population.
- Evaluate the objective function *J* for each candidate.
- Apply RTO operators (growth, pruning, etc.) to explore the search space.
- Select the optimal set of parameters.
- Load the optimized parameters into the controller.

5. IMPLEMENTATION CONSIDERATIONS AND COMPUTATIONAL COMPLEXITY

This section addresses the computational burden of the designed approach. Although the proposed fractional-order proportional-integral feedback regulator (FO-FPI) and its optimization using the RTO algorithm were validated via MATLAB/Simulink simulation, its practical implementation in real-time devices requires careful consideration. The implementation complexity arises mainly from two aspects: achieving a fractional-order controller, and the offline tuning process using the RTO algorithm.

1. Fractional-Order Controller Realization

The utilization of numerical approximation methods is a hallmark of the fractional-order proportional-integral controller's implementation, such as Oustaloup's

recursive approximation, which approximates the fractional operator $s^{\pm\alpha}$ by a rational transfer function within a defined frequency band. The computational complexity of this implementation depends on the approximation order N. For a filter of order N, the controller requires 2N first-order sections, which correspond to 2N additional multiplications and additions per control step. Thus, the computational load increases linearly with N. In practice, values of N between 5 and 10 provide a good trade-off between accuracy and computational burden, making the controller suitable for real-time implementation on standard digital signal processors (DSPs) or microcontrollers.

2. Real-Time Execution and Sampling Requirements

The implementation of the proposed control strategy occurs in real time, executed within the inverter control loop. The required sampling frequency must be sufficiently high to ensure accurate current and power regulation, and to maintain stability under fast transient conditions. In the current study, a sampling frequency of 10–20 kHz is used in simulations, which is compatible with typical DSP-based inverter controllers used in WT systems. The fractional-order filter operations can be executed within the available computation time, provided that the control platform supports fast floating-point arithmetic or fixed-point implementation with adequate precision.

3. Offline Tuning Using RTO Algorithm

The RTO algorithm is employed only during the design phase to determine the optimal FO-FPI gains. Since RTO is an offline optimization process, it does not add any computational burden during real-time operation. Once the optimal parameters are obtained, they are fixed and loaded into the controller. Therefore, the real-time computational load is dominated solely by the fractional-order controller execution and the power estimation block.

4. Hardware Compatibility and Practical Feasibility

The proposed controller is compatible with existing WT converter hardware, as it can be implemented on common industrial platforms such as DSPs (e.g., TI C2000 series), FPGAs, or industrial controllers with sufficient computational capability. The required memory for storing the fractional-order filter coefficients and controller parameters is minimal, and the arithmetic operations are within the capabilities of modern control hardware. For systems with limited computational resources, the fractional-order controller can be implemented using reduced-order approximations or fixed-point arithmetic to reduce processing time and memory usage.

6. COMPUTATIONAL COMPLEXITY SUMMARY

The following paragraph delineates a concise synopsis of the real-time computational cost of the proposed method:

Fractional-order filter operations: O(N) per control step

Power estimation and error calculation: O(1) per control step

PWM generation: O(1) per control step

Overall, the proposed FO-FPI controller can be implemented in real-time using standard control hardware without significantly increasing computational burden compared to conventional PI controllers. Future work will include a detailed hardware-in-the-loop (HIL) implementation and experimental validation to further assess real-time performance and hardware requirements.

7. SIMULATION RESULTS

In this section, the FO-FPI-RTO technique is implemented using MATLAB 2014, in conjunction with the PWM method. A comparative analysis is conducted with the 12 sectors DPC (12-DPC) control method. A comparative analysis is conducted between two algorithms with respect to energy fluctuations, response time, reference tracking, current THD, strength, overshoot value, and SSE of DFIG power. To study the operational performance of the FO-FPI-RTO technique with the PWM method, variable WS profiles are used. A robustness test is also used to examine the strength and efficacy of the new algorithm under varying system parameters. The DFIG and MRWT parameters are listed in Table 3. Some images of the control designed in MATLAB are included in the supplementary file.

The parameters of the DFIG used in this study were selected from standard WT generator models commonly found in scientific literature and represent typical values for multi-megawatt DFIG generators. These parameters were chosen based on their practical relevance, physical realism, and compatibility with the rated power of the MRWT system. It was implemented in a MATLAB/Simulink model to accurately represent the electrical and mechanical dynamics of a DFIG generator. To assess the model's robustness, key parameters such as rotor resistance (R_r) and inductance were varied within realistic ranges to simulate the effects of temperature, magnetic saturation, and parameter uncertainties. This ensures the effectiveness of the proposed control strategy under practical operating conditions.

A. First test: With the MPPT technique

The novel algorithm proposed in this study is implemented using MATLAB, and its performance is compared to the 12-DPC approach. Initially, the variable WSs are employed to assess the efficacy of the

algorithm. The results of the aforementioned test for the two algorithms are presented in Figures 6 and 7.

Table 3. System parameters

	Parameter	Values
DFIG	R_s	12 mΩ
	p	2
	P_{sn}	1500 kW
	R_r	21 mΩ
	L_m	13.5 mH
	L_r	13.6 mH
	J	1000 kg.m^2
	L_s	13.7 mH
	f_r	2.4 mN·m/s
	Vs	380/696 V
	fs	50 Hz
MRWT	Number of turbine blades	3
	R_2	25.5 m
	Number of secondary WT blades	3
	r_2	0.5 m
	r_g	0.75 m
	R_1	13.2 m
	r_1	1 m
	J_2	1000 Kg.m^2
	J_1	500 Kg.m^2

Figure 6a illustrates the WS variations employed in this study to examine the behavior of the novel algorithm. As illustrated in Figure 6b, the variation in the reactive power of two regulators employing the MPPT is evident. This reactive power remains constant and unchanging, regardless of fluctuations in WS. This power has a fast, dynamic response, with response times of 0.021 ms and 2.85 ms for the 12-DPC and FO-FPI-RTO, respectively. Thus, the 12-DPC reduced the reactive power response time by 99.26% compared to the FO-FPI-RTO. Figure 6b shows the presence of reactive power ripples when using both algorithms. These ripples, as shown in Figure 7a, are significantly lower in the FO-FPI-RTO algorithm compared to 12-DPC. The estimated ripple effects for 12-DPC and FO-FPI-RTO are 40,000 VAR and 4,000 VAR, respectively. These values indicate that reactive power ripple is 90% lower in FO-FPI-RTO compared to 12-DPC.

In this test, the SSE and reactive power overshoot values for the 12-DPC model were estimated to be 1416.60 VAR and 5752.60 VAR, respectively. Under the new algorithm, the SSE and reactive power overshoot values were estimated to be 107.50 VAR and 400 VAR, respectively. From these values, it is noted that the new algorithm reduced the SSE and reactive power overshoot values by 92.41% and 93.04%, respectively, compared to the 12-DPC.

As illustrated in Figure 6c, the active power of the two algorithms demonstrates variation in the initial test. It is evident that this power is subject to variation in WS and the presence of ripples. As demonstrated in Figure 7b, the use of the novel algorithm results in a substantial decrease in these ripples compared to 12-DPC. It is noteworthy that this power output exhibits negative values, suggesting that the examined system is expending energy on the grid. In this test, the overshoot, ripples, and SSE values for the 12-DPC strategy were estimated to be 19,330 W, 7,300 W, and 2,850 W, respectively. For the new strategy, the overshoot, ripples, and SSE values were estimated to be 960 W, 1,100 W, and 1,150 W, respectively. Consequently, the novel algorithm diminished the overshoot, ripples, and SSE values by 95.03%, 84.93%, and 59.64%, respectively, in comparison to the 12-DPC strategy. The findings indicated that the response time to active power in this test was estimated at 0.97 milliseconds (ms) and 2.84 ms for the 12-DPC and FO-FPI-RTO algorithms, respectively. These values indicate that the new algorithm offers an unsatisfactory time compared to the 12-DPC algorithm. Consequently, the response time to active power is 65.84% more efficient when the 12-DPC algorithm is employed as opposed to the FO-FPI-RTO algorithm. Consequently, the response time to active power can be regarded as a shortcoming of the novel algorithm in this investigation. This disadvantage can be attributed to the optimal gain values. This drawback could be overcome in the future by implementing alternative strategies, such as the use of NRAX.

Figure 6d illustrates the variation of torque over time for both algorithms. It is important to note that this torque is subject to variation in both WS and the presence of ripples. As demonstrated in Figure 7c, these undulations are reduced in the new algorithm in comparison to the 12-DPC algorithm. The torque fluctuations in this test were estimated to be 50.37 N·m and 14.22 N·m for the 12-DPC and FO-FPI-RTO, respectively. Therefore, the torque ripples are 71.76% lower than those for the 12-DPC. Furthermore, Figure 6d shows that the torques for both algorithms take negative values. These negative values indicate that the generator is in power production mode.

Figure 6e illustrates the variation in current over time for the two algorithms in the initial test case. It has been observed that the current exhibits a direct correlation with the variations in active power and WS for both controls, with the presence of ripples noted. Figure 7d demonstrates that the amplitude of these ripples is diminished when employing the novel algorithm in comparison to the 12-DPC strategy. As demonstrated in

Figure 7d, the current signal latency for both algorithms is equivalent, estimated at 0.02 seconds. In this test, the current fluctuations were estimated at 10 A and 4.50 A for 12-DPC and FO-FPI-RTO, respectively. Consequently, the current ripples are 55% lower than those for 12-DPC. The current ratio indicates that the new algorithm is achieving a satisfactory level of quality, suggesting its potential as a promising solution. Figure 6f represents the power factor variation over time for two regulators using the MPPT. This figure shows that the power factor for both controllers is equal to 1. As shown in Figure 7e, the power factor fluctuations are significantly lower with the new algorithm compared to the 12-DPC.

Figures 6g and 6h illustrate the THD values for the two algorithms employed in this study under the MPPT. According to the aforementioned figures, the THD value was estimated to be 1.90% for the 12-DPC algorithm and 1.80% for the FO-FPI-RTO algorithm. These values indicate that the THD is lower for the FO-FPI-RTO algorithm compared to the 12-DPC strategy. This reduction is estimated to be 5.26% compared to the 12-DPC algorithm. Consequently, this ratio underscores the efficacy of the novel algorithm in enhancing current quality, thereby establishing it as a dependable solution for other applications.

In this particular test, the ITAE values for active power were estimated to be 530.70 W and 102.20 W for the 12-DPC and FO-FPI-RTO, respectively. It is noteworthy that the ITAE values are considerably lower when employing the novel algorithm. This decline can be attributed to the efficacy of the algorithm in question, which has been demonstrated to possess a notable capacity to enhance the characteristics of the system under study. Therefore, it can be concluded that the ITAE value is 80.74% lower when using the new algorithm compared to the 12-DPC.

Although the performance of the proposed control strategy is quantitatively evaluated using percentage-based improvements, these results can be physically interpreted by examining the underlying dynamics of the DFIG-based MRWT system.

The reduction in active and reactive power ripples is primarily attributed to the enhanced damping introduced by the nonlinear fractional-order control action. By modulating the control effort as a function of the error magnitude, the proposed controller mitigates oscillatory behavior arising from electromagnetic coupling and parameter uncertainties, leading to smoother power exchange between the generator and the grid.

The observed improvement in THD can be physically explained by the more continuous and less aggressive switching behavior of the inverter. The nonlinear gain shaping reduces abrupt variations in the control signal, thereby limiting high-frequency current components and improving current waveform quality.

Improvements in robustness under WS variations and parameter mismatches result from the controller's adaptive amplification mechanism. During large disturbances, the nonlinear exponent increases the corrective control effort, compensating for reduced electromagnetic stiffness caused by variations in rotor resistance or inductance. Under steady-state conditions, the control action remains moderate, preventing excessive oscillations.

Thus, the reported percentage improvements are a direct consequence of improved energy flow regulation, enhanced damping, and better coordination between the electrical and mechanical subsystems of the WE conversion system.

B. Second test

In this study, the robustness of the proposed controller was evaluated by varying the resistance of both the stator and rotor. Additionally, the inductance of the rotor and stator was varied using the DFIG. These parameters were chosen due to their high sensitivity to operating conditions, such as temperature variations, magnetic saturation, and machine aging. Increasing the rotor/stator resistance mimics the effects of heating and aging, impacting damping and transient response. Conversely, decreasing inductance represents magnetic saturation and parameter uncertainty, leading to reduced stability and increased oscillations. These changes are essential for evaluating the controller's ability to maintain PQ under realistic operating conditions. Other parameters, such as inertia, are less variable or require changes in devices, and therefore were not included in this study.

This test is completely different from the first test. However, the same WS change pattern is used to study the operational performance of the designed approach. The resistance values are multiplied by 2, while the inductance values are divided by 2. The results of this test are shown in Figures 8 and 9. Despite the variation in generator parameters, the power outputs (Figures 8a and 8b) still follow the reference values well, with a fast dynamic response and undulations. Also, the active power continues to vary with WS variations, which is the same as the results of the first test. Figure 8a shows that the reactive power remains constant and does not vary with WS changes. Figures 9a and 9b show that the power fluctuations in this test have increased significantly compared to the first test. However, this effect is greater when using 12-DPC than when using the new algorithm.

In this test, the values of response time, ripples, SSE, and overshoot of active power for the 12-DPC strategy were estimated to be 0.51 milliseconds (ms), 30,000 watts (W), 6,970 W, and 7,000 W, respectively. The values of response time, ripples, SSE, and overshoot of active power were estimated to be 1.51 milliseconds (ms), 5,000 watts (W), 1,210 W, and 1,000 W, respectively, for the new algorithm. These values

indicate that the algorithm yielded unsatisfactory active power latency compared to 12-DPC. Consequently, the active power latency exhibited a 66.22% enhancement with the 12-DPC algorithm. However, the new algorithm yielded superior values for fluctuations, SSE, and overshoot of active power compared to 12-DPC. The efficacy of the novel algorithm was demonstrated by its ability to reduce undulation, SSE, and overshoot of active power by 83.33%, 82.63%, and 85.71%, respectively, when compared to 12-DPC. The efficacy and robustness of this novel approach in enhancing active power characteristics is evidenced by these figures, thereby establishing it as a reliable solution for a range of industrial applications. Conversely, the response time, ripples, SSE, and overshoot values for reactive power utilizing the 12-DPC algorithm were estimated to be 0.021 ms, 42000 VAR, 5200 VAR, and 7013.50 VAR, respectively. In the new algorithm, the response time, ripples, SSE, and overshoot values for the reactive power were estimated to be 1.48 milliseconds (ms), 8271.20 VAR, 1616 VAR, and 3256.90 VAR, respectively. The findings reveal that the values associated with the ripple, SSE, and overshoot metrics demonstrate a substantial enhancement, with improvements of 80.30%, 68.92%, and 66.93%, respectively, when employing the novel algorithm in comparison to the 12-DPC. However, the new algorithm demonstrates an unsatisfactory power response time in comparison to the 12-DPC. This disadvantage can be attributed to the controller's design gain values. Therefore, it can be concluded that the power response time is an additional disadvantage of the new algorithm in this test.

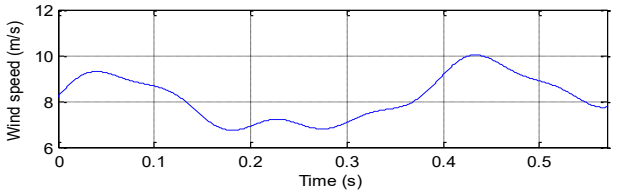

a) WS profile

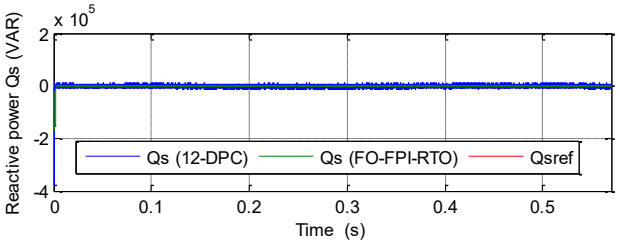

b) *Qs*

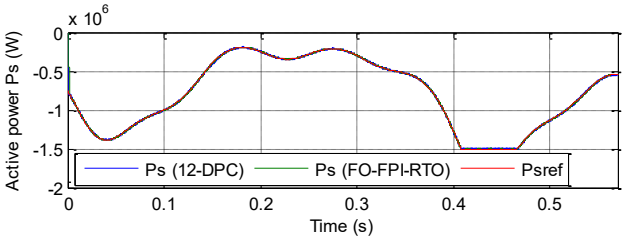

c)*Ps*

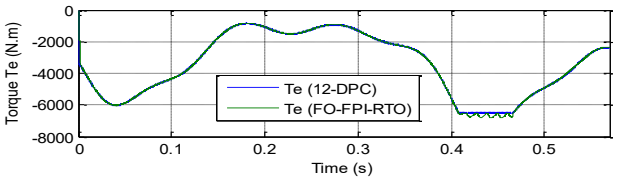

d)Torque.

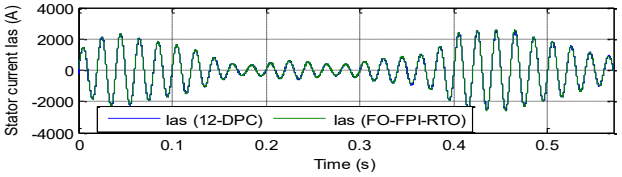

e) Current**.**

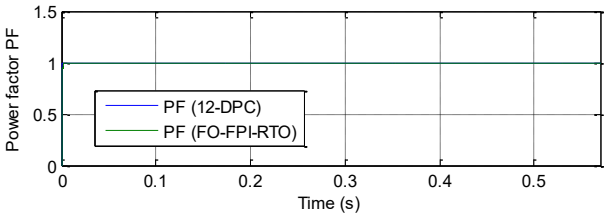

f) Power factor.

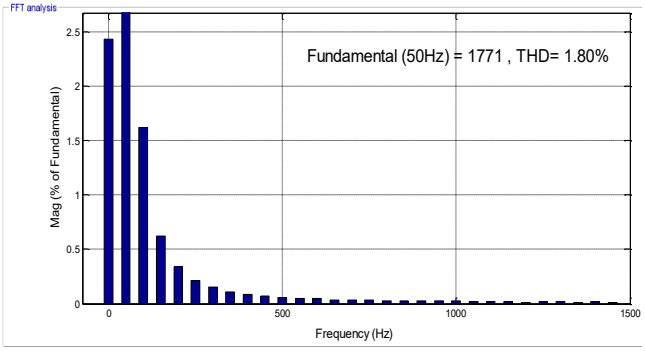

g) Stator current THD (FO-FPI-RTO).

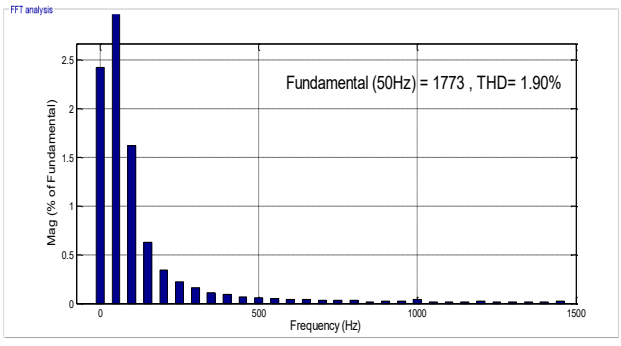

h) Stator current THD (12-DPC).

Figure 6. Simulation results obtained for the first test case under the proposed control strategies.

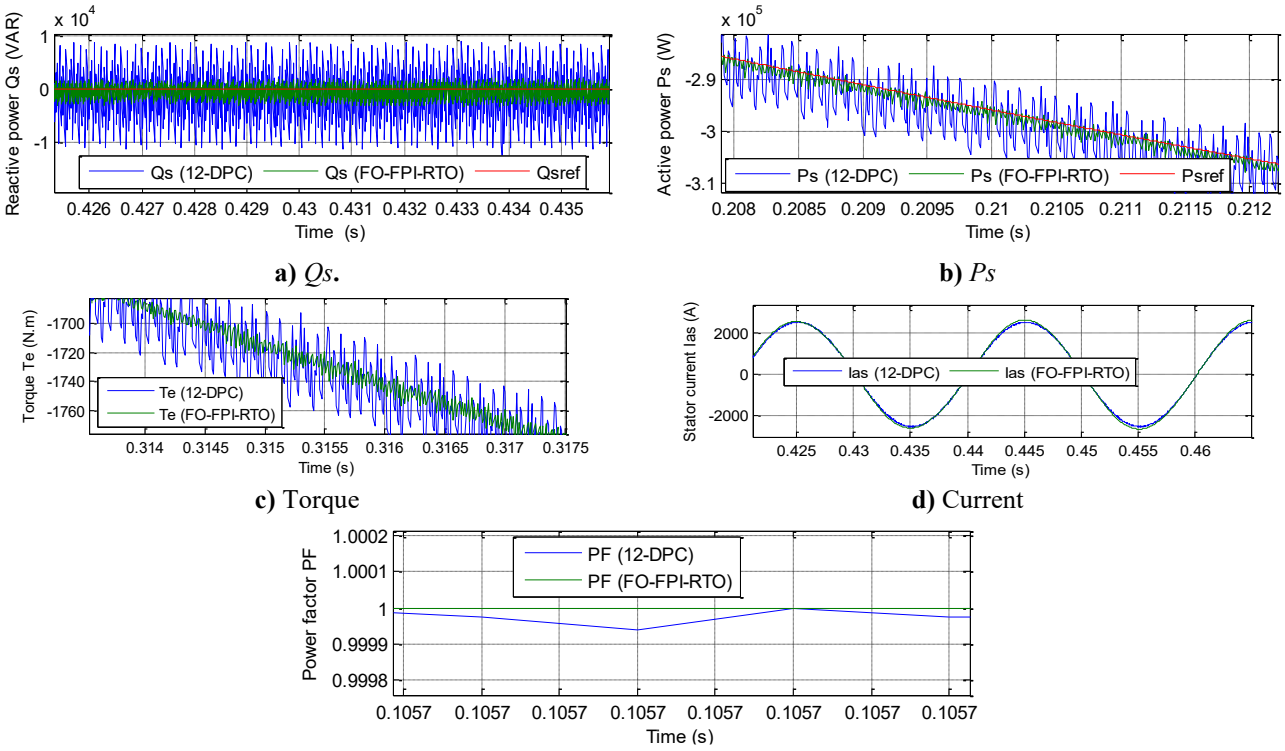

a) *Qs*. **b)** *Ps*

c) Torque **d)** Current

e)Power factor.

Figure 7. Enlarged view of the first test results for improved visualization.

The torque generated by the generator employing the two proposed algorithms is illustrated in Figure 8c. Notwithstanding the variation in generator parameters, the torque continues to vary depending on the active power and the presence of fluctuations. It is noteworthy that the torque remains negative, which is consistent with the outcomes of the initial test. As demonstrated in Figure 9c, the torque fluctuations are considerably reduced with the novel algorithm in comparison to the 12-DPC. In this test, torque fluctuations were estimated at 120 N·m using the 12-DPC method and 25 N·m using the new algorithm. The observed values suggest that the ripple patterns exhibited an increase in this test compared to the initial test, indicating that torque was influenced by alterations in system parameters. The aforementioned ripple phenomenon exhibits a 79.16% decrease in comparison with the ripple phenomenon utilized in conjunction with the 12-DPC method.

The current for both controls is shown in Figure 8d. This current continues to vary with WS, regardless of the machine's parameters. Furthermore, the current has a sinusoidal shape when using both algorithms, with a period of 0.02 seconds, which is the same as the results of the first test. As shown in Figure 9d, the current fluctuations are significantly lower with the new strategy compared to the 12-DPC strategy. These ripples are estimated at 35 A and 3.67 A, respectively. Therefore, the current fluctuations are 89.51% lower than with the 12-DPC.

Figure 8e represents the change in power factor when using both strategies. It is noticeable that despite the system parameters changing, this factor remains equal to 1 when using both controls, indicating the robustness of both approaches. However, according to Figure 9e, the power factor is significantly better when using the new algorithm compared to 12-DPC. These results demonstrate the effectiveness and operational performance of the new algorithm compared to 12-DPC, making it a topic of interest for future research.

The THD values for both controls utilized in this test are displayed in Figures 8f and 8g. According to the available data, the THD was estimated to be 2.16% using the 12-DPC and 1.82% using the new algorithm. These values suggest that the THD is influenced by alterations in machine parameters, resulting in an augmentation of the THD compared to the initial test. This effect is amplified significantly when utilizing the 12-DPC compared to the novel algorithm. Consequently, the new algorithm diminishes the THD by 15.74% compared to the 12-DPC algorithm. The findings indicate the efficacy of the novel algorithm in enhancing the current quality, despite variations in machine parameters, thereby ensuring the reliability of the solution control.

In this experiment, the ITAE value of active power was estimated to be 1.423e+4 W when the 12-DPC was utilized, and 1350 W when the novel algorithm was employed. It is noteworthy that the ITAE value exhibited a substantial increase in this experiment compared to the initial test, suggesting that the ITAE value is influenced by alterations in machine parameters. This effect is amplified significantly when utilizing the 12-DPC as opposed to the FO-FPI-RTO. Consequently, the ITAE value is considerably lower

when using the new algorithm compared to the 12-DPC. This decline in ITAE value is estimated at 90.51%. This percentage is indicative of the efficacy and solidity of the new algorithm in enhancing system properties.

The reduction of power ripples and THD achieved by the proposed FO-FPI-RTO controller can be explained by the combined effects of nonlinear gain shaping, improved power error regulation, and smoother inverter switching behavior.

First, the fractional-order feedback structure introduces a memory effect in the control loop, which smooths the evolution of the power error signal. Unlike conventional integer-order PI or 12-sector DPC strategies that rely on abrupt switching decisions, the proposed controller generates a more continuous control signal. This continuity limits sudden variations in the inverter voltage commands, thereby reducing high-frequency oscillations in stator and rotor currents.

Second, the nonlinear power-law term modulates the control effort according to the magnitude of the power error. For large deviations caused by WS fluctuations or parameter uncertainties, the controller provides strong corrective action, ensuring rapid attenuation of oscillations. For small SSEs, the control action is naturally softened, which prevents over-correction and suppresses residual power ripples.

Third, the optimized controller gains obtained through the RTO algorithm ensure balanced tuning between proportional and integral actions. This tuning improves decoupling between active and reactive power channels, reducing cross-coupling effects that are a major source of power oscillations in conventional DPC schemes.

Finally, the use of PWM in conjunction with the proposed controller leads to a fixed switching frequency operation. Compared to hysteresis-based 12-sector DPC, this significantly reduces current distortion by avoiding variable switching frequency and discontinuous voltage vectors, resulting in lower THD.

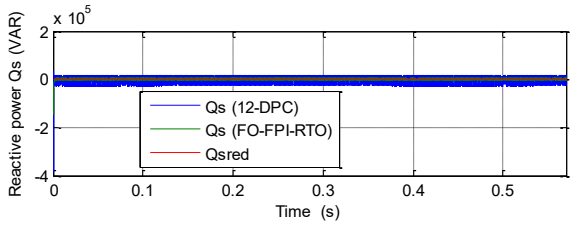

a)*Qs*

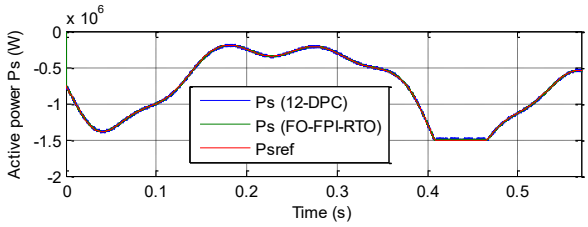

b)*Ps*

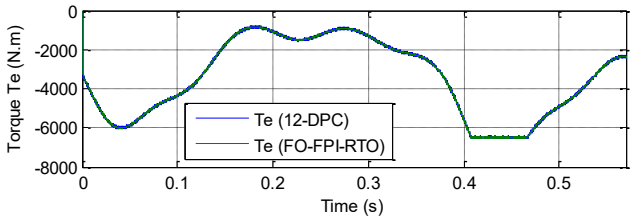

c) Torque.

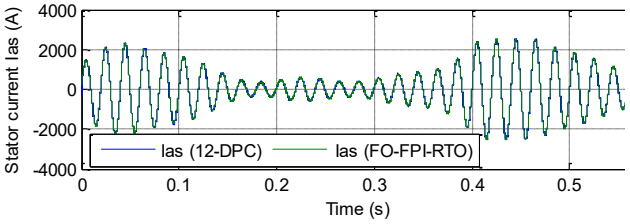

d)Current**.**

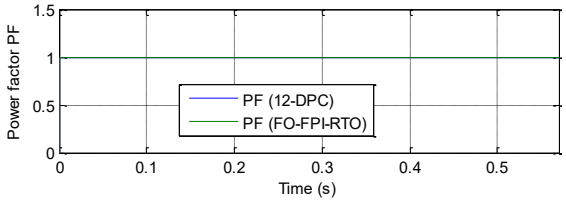

e)Power factor.

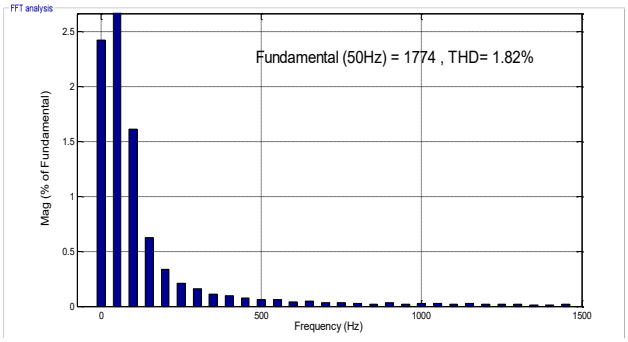

f)Stator current THD(FO-FPI-RTO).

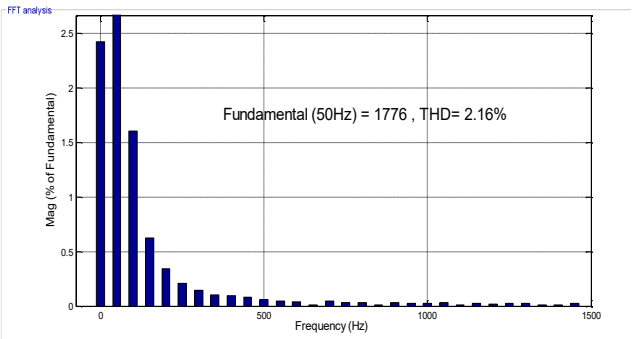

g)Stator current THD(12-DPC).

Figure 8. Results of the second test case: (a) active power response, (b) reactive power response, (c) Torque, (d) stator current waveform, (e) Power factor, (f) Stator current THD (FO-FPI-RTO), and (g) Stator current THD (DPC).

Overall, the observed reductions in power ripples and THD are the direct consequence of smoother power regulation, enhanced damping, and improved inverter switching characteristics introduced by the FO-FPI-RTO control strategy.

8. ROBUSTNESS–RESPONSE TIME TRADE-OFF ANALYSIS

The proposed FO-FPI-RTO controller shows improved robustness under parameter variations but slower dynamic response compared to the 12-sector DPC approach. This behavior can be understood through the underlying structure of the controller and the role of the nonlinear exponent α.

1) *Why Robustness Improves*

The FO-FPI-RTO controller includes a nonlinear fractional term that introduces additional damping and memory effect, making the system less sensitive to parameter variations.

Mathematically, the closed-loop error dynamics can be approximated as:

$$\dot{e}(t) = -(K_1.e + K_2.z)^{\alpha} \quad (42)$$

Where, $z(t) = \int E(t).dt$.

The nonlinear exponent α>1 increases control effort during large deviations, leading to:

- Stronger correction during disturbances,
- Reduced oscillation amplitude,
- Improved tolerance to parameter mismatch.

This effect increases robustness but also increases the "effective damping" of the system.

2) *Why Response Time Slows Down*

In control systems, increased damping usually reduces oscillation but increases settling time. This is a classical trade-off.

In the proposed controller:

- The fractional power term reduces aggressive control actions when the error is small.
- The controller becomes less "reactive" during fast transient conditions.
- As a result, the system exhibits slower convergence, as observed in the simulation results.
- This explains why the response time is longer than 12-DPC.

Observation: 12-DPC achieves faster t_s but higher ΔP and THD.

FO-FPI-RTO yields lower ΔP and THD but larger t_s.

3) *Practical Acceptability*

The trade-off is acceptable in WE systems for the following reasons:

- Power quality is prioritized over response speed because WS variations are slow compared to electrical dynamics.
- High robustness is required to tolerate parameter variations and grid disturbances.
- The system does not require ultra-fast response as in high-speed drives.
- Thus, the increased response time is a reasonable compromise.

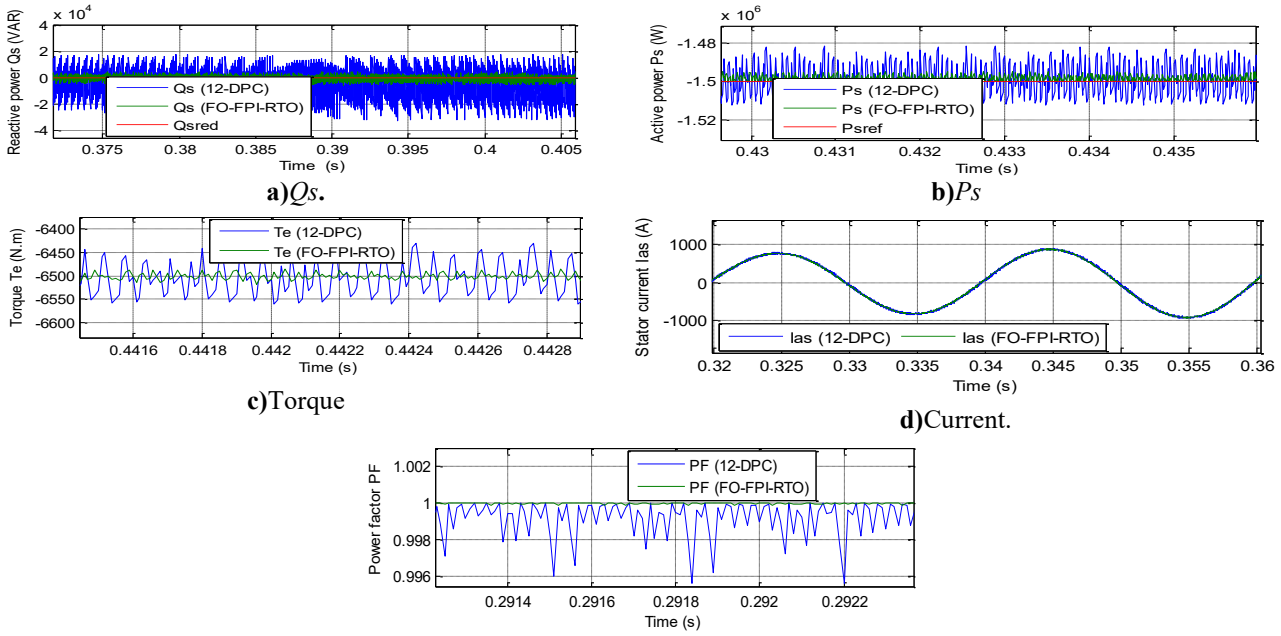

a)*Qs*. **b)***Ps*

c)Torque **d)**Current.

e)Power factor.

Figure 9. Zoomed view of the second test results.

9. POTENTIAL IMPROVEMENTS

To mitigate the slower response while preserving robustness, the following strategies can be considered:

- Gain scheduling based on operating conditions
- Hybrid control combining FO-FPI-RTO during steady state and 12-DPC during transients
- Adaptive α tuning (dynamic adjustment of α)

- Higher-order optimization to reduce settling time while maintaining robustness
- These strategies are recommended as future work.

Table 4 compares the obtained overshoot power reductions with related works. The comparison is based on the results of the first test of the new algorithm. Table 4 demonstrates the new algorithm's superiority over several existing studies in the literature, yielding a significantly higher overshoot power reduction. This superiority is due to its effectiveness, high efficiency, and robustness, which distinguish it from other strategies. According to Table 4, the new algorithm improved reduction ratios for overshoot of active power by 82.16%, 29.17%, 46.75%, 34.51%, and 93.07% (Test 1), respectively, compared to works [51], [52], [55], [56], and [58], respectively. Furthermore, the proposed new approach improves reduction ratios for the overshoot of reactive power by 92.39%, 25.32%, 7.83%, 28.71%, and 73.61%, compared to works [51], [52], [55], [56], and [58], respectively. Moreover, Table 4 shows that the greatest improvement rate in the case of active power was compared to work [58], where this rate was estimated at 93.49% (first test). In the case of reactive ability, the greatest improvement rate was compared to work [51], where this rate was estimated at 92.39%.The lowest improvement rate obtained in the case of active power was compared to work [52], where this rate was estimated at 29.17%. In the case of reactive power, the lowest improvement rate was estimated at 22.26%, where this rate was obtained compared to work [57].

These improvements demonstrate the significant strength of the new algorithm, making it a promising solution.

Table 4. Comparison of the proposed FO-FPI-RTO controller's overshoot reduction with results reported in recent literature.

Refs.		Minimization rates		Improvements (%)	
		Qs	***Ps***	***Ps (W)***	***Qs* (VAR)**
[51]		16.59%	7.23%	82.16	92.39
[52]		65.90%	70.96%	29.17	25.32
[53]		80.07%	50.68%	46.66	13.94
[54]	Test 1	44.06%	32.20%	52.64	66.11
	Test 2	22.77%	32.49%	75.52	65.81
[55]		85.75%	50.59%	46.75	7.83
[56]		60.93%	67.74%	34.51	28.71
[57]	Test 1	48.38%	73.87%	48	22.26
	Test 2	49.32%	20.10%	46.99	78.84
[58]	Test 1	6.44%	25.07%	93.07	73.61
	Test 2	6.05%	9.19%	93.49	90.23
New algorithm	Test 1	**93.04**%	95.03%	-	

10. DISCUSSION

The simulation results demonstrate that the proposed FO-FPI-RTO controller significantly improves PQ and robustness compared to conventional 12-sector DPC. These improvements can be explained by the intrinsic properties of fractional-order control, particularly the memory effect and smoothing behavior, as well as the nonlinear gain modulation introduced by the exponent α.

10.1 Memory Effect and Smoothing Properties

Fractional-order controllers inherently possess a memory property, meaning that the control action depends not only on the current error but also on the historical evolution of the error signal. In the proposed control law, the fractional exponent applied to the integrated error results in a control action that accumulates past information and smooths transient variations. This memory effect reduces abrupt changes in the control signal and consequently limits high-frequency oscillations in the inverter switching controls. As a result, the system exhibits:

Reduced power ripples due to smoother regulation of active/reactive power.

Lower THD, as the inverter switching becomes less aggressive and more continuous compared to 12-sector DPC.

Improved damping, which helps to stabilize the system under parameter variations.

10.2 Robustness Improvement

The robustness enhancement under parameter variations (e.g., changes in rotor resistance and inductance) is primarily due to the nonlinear damping effect produced by the fractional exponent α. When the system experiences large disturbances or parameter mismatch, the control action is automatically amplified, providing stronger correction. Conversely, during steady-state operation, the control action is moderated to avoid unnecessary oscillations. This behavior is

consistent with the observed reduction in power ripple and improved stability under uncertainty.

10.3 Practical Trade-offs

The improved robustness and reduced ripple come at the cost of slower response time. This trade-off is typical in control systems where increased damping reduces oscillations but increases settling time. In the context of WE systems, this trade-off is acceptable for the following reasons:

Wind speed variations occur over seconds, whereas electrical dynamics occur over milliseconds. Therefore, a slightly slower electrical response does not significantly affect overall system performance.

Power quality and stability are prioritized over ultra-fast response in grid-connected WTs.

The reduced THD and power ripple improve grid compliance and reduce stress on electrical components.

10.4 Implementation Considerations

Although the current study is based on MATLAB simulations, the fractional-order operator can be implemented using rational approximation methods such as the Oustaloup recursive filter. The approximation order and frequency range should be chosen to balance accuracy and computational cost. Real-time implementation on DSP or FPGA platforms is feasible, but it requires careful consideration of sampling frequency and filter order to avoid excessive computational load.

10.5 Summary of Key Insights

In summary, the proposed FO-FPI-RTO controller leverages fractional-order memory and smoothing properties to improve PQ and robustness. The trade-off between response time and robustness is justified for WE applications, where stable and smooth power delivery is more critical than ultra-fast dynamic response. These findings provide a clear physical interpretation of the simulation results and support the practical relevance of the proposed approach.

11. LIMITATIONS AND FUTURE WORK

Although the proposed fractional-order DPC strategy optimized using the RTO algorithm demonstrates promising performance in improving power and current quality, several limitations of the present study should be acknowledged. First, the validation of the proposed method is limited to MATLAB-based simulations, and no experimental or hardware-in-the-loop implementation is provided. Consequently, practical issues such as measurement noise, parameter uncertainties, computational delays, and real-time implementation constraints are not fully addressed.

Second, the proposed control strategy is applied only to the machine-side inverter of the DFIG system. The interaction with other system components, particularly the GSC and overall wind farm dynamics, is not considered, which restricts the general applicability of the approach at the system level.

Moreover, the controller performance relies on accurate power estimation and on the optimal tuning of the fractional-order PI parameters using the RTO algorithm. Any inaccuracies in power estimation or variations in system parameters may affect the control effectiveness. In addition, although fractional-order controller's offer enhanced robustness, their implementation complexity in real-time digital control platforms has not been investigated in this work.

Future research will focus on experimental validation of the proposed method using hardware-in-the-loop and laboratory-scale test benches to assess its practical feasibility. Extending the control strategy to include the grid-side converter, investigating its behavior under grid disturbances and fault conditions, and comparing it with other advanced control techniques are also important directions for future work. Furthermore, adaptive or hybrid control strategies may be explored to enhance dynamic response while preserving robustness and PQ improvements.

12. CONCLUSIONS

This paper investigates the effectiveness of a designed algorithm in enhancing the power and current quality of a DFIG in a multi-rotor turbine system. The operational performance is then compared with that of a 12-DPC algorithm. The comparative results demonstrate that the new algorithm exhibits superior performance in terms of output PQ by reducing power ripples. Specifically, the novel approach exhibited superior performance in mitigating current and torque ripples, reducing them in the variable WS test by 55% and 71.76%, respectively. In addition, the THD of current and ITAE values were reduced by 5.26% and 80.74%, respectively, in comparison with the 12-DPC. In the event of a variation in generator parameters, the new algorithm reduced current and torque ripples by 89.51% and 79.16%, respectively, compared to the conventional approach. In addition, the novel algorithm has been demonstrated to reduce the overshoot of active power by 85.71% in comparison with traditional methodologies. The results of the tests indicated the reliability and efficacy of the novel algorithm in enhancing the features of the multi-rotor turbine system under investigation. This work offers significant insights into enhancing the quality of energy and current, thereby contributing to the enhancement of the reliability of WE systems.

Nomenclature

FPI	Feedback proportional-integral regulator
DTC	Direct torque control
WT	Wind turbine
MPPT	Maximum power point tracking
RTO	Rooted tree optimization
FOPI	Fractional-order proportional-integral controller
ANN	Artificial neural network
PSO	Particle swarm optimization
FL	Fuzzy logic
PI	Proportional-integral regulator
WE	Wind energy
DR	Dynamic response
Ω	Speed
$V_{\alpha s}$ and $V_{\beta s}$	Voltages of the stator in the α-β reference frame
$I_{\alpha s}$ and $I_{\beta s}$	Stator currents in the α-β reference frame
$\varphi_{\alpha r}$ *and* $\varphi_{\beta r}$	Flux of the stator in the α-β reference frame
$\varphi_{\alpha s}$ *and* $\varphi_{\beta s}$	Flux of the stator in the α-β reference frame
BC	Backpropagation controller
DPC	Direct power control
THD	Total harmonic distortion
WS	Wind speed
12-DPC	12-sector direct power control
MRWT	Multi-rotor wind turbine
PQ	Power quality
FOC	Field-oriented control
SMC	Sliding mode control
f	Friction coefficient
J	Inertia torque
p	Pair of poles
SSE	Steady-state error
R_r *and* R_s	Rotor and stator resistance
M	Mutual inductor
L_r *and* L_s	Rotor and stator inductances
T_{em}	Electromagnetic torque
C_p	Power coefficient
ρ	Air density
σ	Dispersion coefficient
C_T	Constant coefficient
K_1, K_2, K_3	Controller gains
α	Fractional-order control gain

REFERENCES

[1] Y. L. A. Sumanth, L. Lakshminarasimman, and R. G. Sambasiva, "Optimal design of FoPID controller for DFIG based wind energy conversion system using Grey-Wolf optimization algorithm," Int. J. Renew. Energy Res., vol. 12, no. 4, pp. 2111–2120, 2022, doi: 10.20508/ijrer.v12i4.13446.g8594.

[2] M. Chakib, N. Tamou, and E. Ahmed, "Contribution of variable speed wind turbine generator based on DFIG using ADRC and RST controllers to frequency regulation," Int. J. Renew. Energy Res., vol. 11, no. 1, pp. 320–331, 2021, doi: 10.20508/ijrer.v11i1.11762.g8136.

[3] K. G. Sanjeev, M. Sundram, and S. Madhu, "Performance enhancement of DFIG based grid connected SHPP using ANN controller," Int. J. Renew. Energy Res., vol. 9, no. 3, pp. 1165–1179, 2019, doi: 10.20508/ijrer.v9i3.9427.g7694.

[4] N. Mohamed, E. Ahmed, and N. Tamou, "Comparative analysis between PI & backstepping control strategies of DFIG driven by wind turbine," Int. J. Renew. Energy Res., vol. 7, no. 3, pp. 1307–1316, 2017, doi: 10.20508/ijrer.v7i3.6066.g7163.

[5] M. Chakib, "A comparative study of PI, RST and ADRC control strategies of a doubly fed induction generator based wind energy conversion system," Int. J. Renew. Energy Res., vol. 8, no. 2, pp. 964–973, 2018, doi: 10.20508/ijrer.v8i2.7645.g7383.

[6] H. Mohamed, K. Nadir, M. Samir, and K. Selman, "Neural network based field oriented control for doubly-fed induction generator," Int. J. Smart Grid, vol. 2, no. 3, pp. 183–187, 2018, doi: 10.20508/ijsmartgrid.v2i3.18.g18.

[7] Ch. R. Reddy, K. Naresh, R. P. Umapathi, and P. Sujatha, "Control of DFIG based wind turbine with hybrid controllers," Int. J. Renew. Energy Res., vol. 10, no. 3, pp. 1488–1500, 2020, doi: 10.20508/ijrer.v10i3.11010.g8028.

[8] R. Zahra, R. Mansour, and A. Mohammadreza, "A new control strategy based on reference values changing for enhancing LVRT capability of DFIG in wind farm," Int. J. Renew. Energy Res., vol. 9, no. 4, pp. 1626–1637, 2019, doi: 10.20508/ijrer.v9i4.9952.g7765.

[9] F. Mohammed, E. Ahmed, N. Mohamed, and N. Tamou, "Control and optimization of a wind energy conversion system based on doubly-fed induction generator using nonlinear control strategies," Int. J. Renew. Energy Res., vol. 9, no. 1, pp. 44–45, 2019, doi: 10.20508/ijrer.v9i1.8812.g7619.

[10] M. Mihir and M. Bhinal, "Modified rotor flux estimated direct torque control for double fed induction generator," Int. J. Renew. Energy Res., vol. 12, no. 1, pp. 124–133, 2022, doi: 10.20508/ijrer.v12i1.12615.g8380.

[11] S. M., E. Ahmed, N. Tamou, and B. I. Badr, "An efficient nonlinear backstepping controller approach of a wind energy conversion system based on a DFIG," Int. J. Renew. Energy Res., vol. 7, no. 4, pp. 1520–1528, 2017, doi: 10.20508/ijrer.v7i4.6112.g7192.

[12] B. D., B. P., D. M., V. K., and D. O., "Artificial intelligence based vector control of induction generator without speed sensor for use in wind energy conversion system," Int. J. Renew. Energy Res., vol. 5, no. 1, pp. 299–307, 2015, doi: 10.20508/ijrer.v5i1.2030.g6498.

[13] Z. Xu, X. Xin, Y. Wang, and J. Wang, "A DFIG low- and high-voltage cascading failure through strategy based on GSC and RSC joint control," Int. J. Electr. Power Energy Syst., vol. 170, p. 110875, 2025, doi: 10.1016/j.ijepes.2025.110875.

[14] Y. S., S. T., S. L. B., M. B., Y. B., A. R. S., M. F. El-N., and S. K., "Effectiveness analysis of twelve sectors of DTC based on a newly modified switching table implemented on a wind turbine DFIG system under variable wind velocity," Ain Shams Eng. J., vol. 14, no. 11, p. 102221, 2023, doi: 10.1016/j.asej.2023.102221.

[15] L. D., H. Caballero-Barragán, L. P. Osuna-Ibarra, E. N. S., and A. G. Loukianov, "Neural sliding mode control of a DFIG based wind turbine with measurement delay," IFAC-PapersOnLine, vol. 51, no. 13, pp. 456–461, 2018, doi: 10.1016/j.ifacol.2018.07.320.

[16] Y. Zhang, Z. Ma, and Z. Wang, "An improved fuzzy logic based DC-link voltage control strategy for smoothing output power of

the PMSG-WECS," Energy Rep., vol. 8, pp. 8413–8425, 2022, doi: 10.1016/j.egyr.2022.06.049.
[17] H. Itouchene, Z. Boudries, and F. Amrane, "Improved power control based variable speed wind-turbine DFIG under hard work conditions: Application of sliding mode theory," Period. Polytech. Electr. Eng. Comput. Sci., 2024, doi: 10.3311/ppee.36760.
[18] K. F. Sayeh, S. Tamalouzt, D. Ziane, A. Bekhiti, Y. Belkhier, "Utilizing fuzzy logic control and neural networks based on artificial intelligence techniques to improve power quality in doubly fed induction generator-based wind turbine system," Int. J. Energy Res., 2025, doi: 10.1155/er/5985904.
[19] A. E., A. I., A. Abdellatif, and S. Shaaban, "Aerodynamic performance and structural design of 5 MW multi rotor system wind turbines," Int. J. Renew. Energy Res., vol. 12, no. 3, pp. 1495–1505, 2022, doi: 10.20508/ijrer.v12i3.13343.g8535.
[20] A. Elkodama et al., "Investigation into the yaw control of a twin-rotor 10 MW wind turbine," Appl. Sci., vol. 14, p. 9810, 2024, doi: 10.3390/app14219810.
[21] H. Benbouhenni et al., "Direct power control based on modified sliding mode controller for a variable-speed multi-rotor wind turbine system using PWM strategy," Energies, vol. 15, p. 3689, 2022, doi: 10.3390/en15103689.
[22] E. Ercan, S. Selim, and F. C. B., "Analysis model of a small scale counter-rotating dual rotor wind turbine with double rotational generator armature," Int. J. Renew. Energy Res., vol. 8, no. 4, pp. 1849–1858, 2018, doi: 10.20508/ijrer.v8i4.8235.g7549.
[23] H. Benbouhenni, I. Colak, and N. Bizon, "Power regulation of variable speed multi rotor wind systems using fuzzy cascaded control," Sci. Rep., vol. 14, p. 16415, 2024, doi: 10.1038/s41598-024-67194-4.
[24] S. Li, X. Chen, Y. Zhang, Y. Wang, and D. Li, "Effect of yaw on aerodynamic performance of co-planar multi-rotor wind turbines," Ocean Eng., vol. 279, p. 114441, 2023, doi: 10.1016/j.oceaneng.2023.114441.
[25] G. Kamyab, "Different options for multi-rotor wind turbine grid connection," J. Eng., vol. 2019, no. 17, pp. 4065–4068, 2019, doi: 10.1049/joe.2018.8009.
[26] E. Aboubakr et al., "LVRT control strategy of DFIG based wind turbines combined the active and passive protections," Int. J. Renew. Energy Res., vol. 7, no. 3, pp. 1258–1269, 2017, doi: 10.20508/ijrer.v7i3.6014.g7159.
[27] R. L. and S. Lekhchine, "Fuzzy logic controller-based power control of DFIG based on wind energy systems," Int. J. Smart Grid, vol. 8, no. 1, pp. 74–80, 2024, doi: 10.20508/ijsmartgrid.v8i1.334.g346.
[28] O. Kenneth, "A variable speed wind turbine flywheel based coordinated control system for enhancing grid frequency dynamics," Int. J. Smart Grid, vol. 2, no. 2, pp. 123–134, 2018, doi: 10.20508/ijsmartgrid.v2i2.22.g158.
[29] M. Nadour, A. Essadki, and T. Nasser, "Comparative analysis between PI & backstepping control strategies of DFIG driven by wind turbine," Int. J. Renew. Energy Res., vol. 7, no. 3, pp. 1307–1316, 2017, doi: 10.20508/ijrer.v7i3.6066.g7163.
[30] K. Xiahou, M. S. Li, Y. Liu and Q. H. Wu, "Sensor Fault Tolerance Enhancement of DFIG-WTs via Perturbation Observer-Based DPC and Two-Stage Kalman Filters," in IEEE Transactions on Energy Conversion, vol. 33, no. 2, pp. 483-495, June 2018, doi: 10.1109/TEC.2017.2771250.
[31] K. G. Sanjeev, M. Sundram, and S. Madhu, "Performance enhancement of DFIG based grid connected SHPP using ANN controller," Int. J. Renew. Energy Res., vol. 9, no. 3, pp. 1165–1179, 2019, doi: 10.20508/ijrer.v9i3.9427.g7694.
[32] Y. B. and D. B. A., "Comparison study between SVM and PWM inverter in sliding mode control of active and reactive power control of a DFIG for variable speed wind energy," Int. J. Renew. Energy Res., vol. 2, no. 3, pp. 471–476, 2012, doi: 10.20508/ijrer.v2i3.269.g6047.
[33] F. Mohammed, E. Ahmed, and N. Tamou, "Comparative analysis between robust SMC & conventional PI controllers used in WECS based on DFIG," Int. J. Renew. Energy Res., vol. 7, no. 4, pp. 2151–2161, 2017, doi: 10.20508/ijrer.v7i4.6441.g7267.
[34] A. K., N. K., and M. F. M., "Wind energy conversion system using DFIG controlled by backstepping and sliding mode strategies," Int. J. Renew. Energy Res., vol. 2, no. 3, pp. 421–430, 2012, doi: 10.20508/ijrer.v2i3.249.g6040.
[35] R. R. Hete et al., "Design and development of PI controller for DFIG grid integration using neural tuning method ensembled with dense plexus terminals," Sci. Rep., vol. 14, p. 7916, 2024, doi: 10.1038/s41598-024-56904-7.
[36] R. Zahra, R. Mansour, and A. Mohammadreza, "A new control strategy based on reference values changing for enhancing LVRT capability of DFIG in wind farm," Int. J. Renew. Energy Res., vol. 9, no. 4, pp. 1626–1637, 2019, doi: 10.20508/ijrer.v9i4.9952.g7765.
[37] M. Amer, A. Miloudi, and F. Lakdja, "Optimal DTC control strategy of DFIG using variable gain PI and hysteresis controllers adjusted by PSO algorithm," Period. Polytech. Electr. Eng. Comput. Sci., vol. 64, no. 1, pp. 74–86, 2020, doi: 10.3311/PPee.14237.
[38] G. Hamza et al., "Using the proportional dual integral strategy to improve the characteristics of the indirect field-oriented control of DFIG-based wind turbine systems," e-Prime – Adv. Electr. Eng. Electron. Energy, vol. 9, p. 100749, 2024, doi: 10.1016/j.prime.2024.100749.
[39] A. M. A. Saad et al., "Optimization of PID controller for hybrid renewable energy system using adaptive sine cosine algorithm," Int. J. Renew. Energy Res., vol. 10, no. 2, pp. 669–677, 2020, doi: 10.20508/ijrer.v10i2.10685.g7938.
[40] A. D. Asma et al., "Robust fractional PI controller design for stand-alone microgrid under load variation: An optimization-based approach," Int. J. Renew. Energy Res., vol. 13, no. 4, pp. 1526–1537, 2023, doi: 10.20508/ijrer.v13i4.14540.g8826.
[41] S. Sahoo, E. Rajsekhar, and P. S. Puhan, "Design and simulation of a GA optimized variable speed DFIG based wind turbine using MATLAB," in Proc. Int. Conf. Intell. Control. Comput. Smart Power (ICICCSP), Hyderabad, India, 2022, pp. 1–4, doi: 10.1109/ICICCSP53532.2022.9862453.
[42] H. Benbouhenni and H. Gasmi, "Comparative study of synergetic controller with super twisting algorithm for rotor side inverter of DFIG," Int. J. Smart Grid, vol. 6, no. 4, pp. 144–156, 2022, doi: 10.20508/ijsmartgrid.v6i4.265.g228.
[43] R. A. J. Amalorpavaraj, P. Kaliannan, S. Padmanaban, U. Subramaniam and V. K. Ramachandaramurthy, "Improved Fault Ride Through Capability in DFIG Based Wind Turbines Using Dynamic Voltage Restorer With Combined Feed-Forward and Feed-Back Control," in IEEE Access, vol. 5, pp. 20494-20503, 2017, doi: 10.1109/ACCESS.2017.2750738.
[44] M. Said et al., "ANT-colony optimization-direct torque control for a doubly fed induction motor: An experimental validation," Energy Rep., vol. 8, pp. 81–98, 2022, doi: 10.1016/j.egyr.2021.11.239.
[45] S. Boubzizi et al., "Comparative study of three types of controllers for DFIG in wind energy conversion system," Prot. Control Mod. Power Syst., vol. 3, p. 21, 2018, doi: 10.1186/s41601-018-0096-y.
[46] M. E. B. Aguilar et al., "Multi-objective PSO for control-loop tuning of DFIG wind turbines with chopper protection and reactive-current injection," Energies, vol. 17, p. 28, 2024, doi: 10.3390/en17010028.
[47] B. Habib, "Rotor flux and electromagnetic torque regulation of DFIG using dual PI controllers," Int. J. Smart Grid, vol. 7, no. 4, pp. 227–234, 2023, doi: 10.20508/ijsmartgrid.v7i4.308.g311.
[48] Z. Dalal et al., "Field-oriented control based on parallel proportional–integral controllers of induction motor drive," Energy Rep., vol. 9, pp. 4846–4860, 2023, doi: 10.1016/j.egyr.2023.04.008.

[49] F. Mazouz, B. Sebti, and I. C., "DPC-SVM of DFIG using fuzzy second order sliding mode approach," Int. J. Smart Grid, vol. 5, no. 4, pp. 174–182, 2021, doi: 10.20508/ijsmartgrid.v5i4.219.g178.

[50] G. Reza, M. Ali, and D. S. Alireza, "A new control algorithm method based on DPC to improve power quality of DFIG in unbalance grid voltage conditions," Int. J. Renew. Energy Res., vol. 8, no. 4, pp. 2228–2238, 2018, doi: 10.20508/ijrer.v8i4.8583.g7527.

[51] I. Sami et al., "A super twisting fractional order terminal sliding mode control for DFIG-based wind energy conversion system," Energies, vol. 13, p. 2158, 2020, doi: 10.3390/en13092158.

[52] B. Habib et al., "HIL test verification of PDPI control of induction generator-based multi-rotor wind turbine systems," Energy Sci. Eng., vol. 13, no. 1, pp. 140–159, 2025, doi: 10.1002/ese3.1976.

[53] H. Benbouhenni and N. Bizon, "Implementation of Robust Fractional-Order Neural Modified Sliding Mode Controls for Managing the Power Output of Doubly Fed Induction Generators," Artificial Intelligence Research and Applications, vol. 1, no. 4, pp. 157–188, 2025, doi: 10.20508/wehhd131.

[54] M. Yessef et al., "Real-time validation of intelligent super twisting sliding mode control for variable-speed DFIG using dSPACE 1104 board," IEEE Access, vol. 12, pp. 31892–31915, 2024, doi: 10.1109/ACCESS.2024.3367828.

[55] H. Benbouhenni and N. Bizon, "Genetic Algorithm–Optimized Cascaded Fractional-Order PI Control for Performance and Power Quality Enhancement of a 1.5 MW DFIG-Based MRWT," Electronics, vol. 15, no. 8, p. 1574, 2026, doi: 10.3390/electronics15081574.

[56] B. Habib et al., "Backstepping control for multi-rotor wind power systems," Majlesi J. Energy Manag., vol. 11, 2023.

[57] B. Habib et al., "A new PI(1 + PI) controller to mitigate power ripples of a variable-speed dual-rotor wind power system using direct power control," Energy Rep., vol. 10, 2023, doi: 10.1016/j.egyr.2023.10.007.

[58] H. Benbouhenni, N. Bizon, and I. Colak, "Super-twisting hysteresis controller for multi-rotor wind energy systems," Int. J. Electron., vol. 112, no. 3, pp. 453–472, 2024, doi: 10.1080/00207217.2024.2312086.